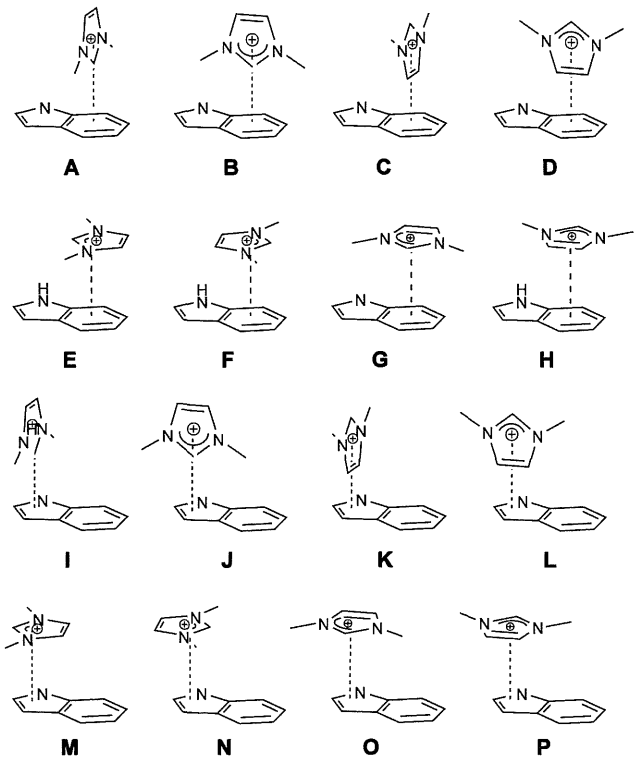

Figure 2. Geometries of indole/imidazolium complexes **A**–**P** used for calculations of interaction energy potentials.

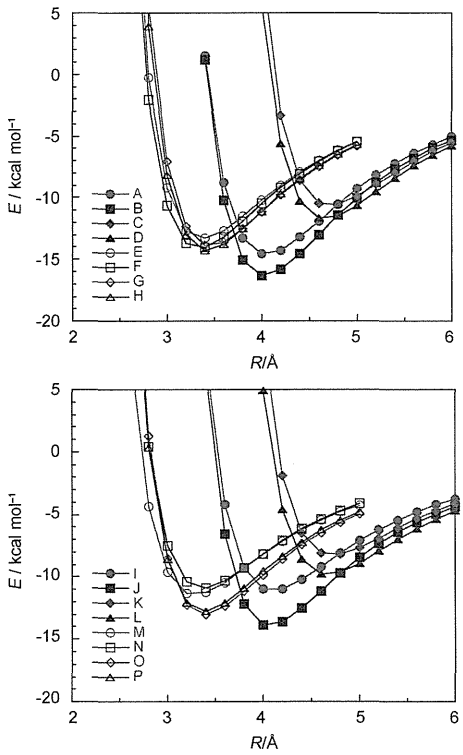

Figure 3. MP2/cc-pVTZ interaction energy potentials for indole/imidazolium complexes **A**-**P** (Figure 2). Intermolecular distance (R) is the distance between the indole plane and the midpoint of the two nitrogen atoms of imidazolium.

for the interaction energy for the geometries **A**–**H**, in which the imidazolium ring locates above the six-membered ring of indole, to be larger than in the corresponding geometries **I**–**P**, in which the imidazolium ring is located above the five-membered ring of indole, which indicates that 1,3-dimethylimidazolium cation prefers to interact with the six-membered ring of indole. These results are consistent with the optimized structure for the indole/Na^+ complex, in which the sodium cation is positioned on the six-membered ring of indole.[1,25] Interestingly, the interaction energy in the complexes (**A**, **B**, **I**, and **J**), in which the C2–H bond of the imidazolium ion points toward the indole, is larger than that of the corresponding complexes (**C**, **D**, **K**, and **L**), in which the C4–H and C5–H bonds of imidazolium have contact with the indole. In particular, the T-shaped structure **B** has a very large interaction energy compared with those of the other structures.

Two stable geometries were obtained by geometry optimization of the indole/1,3-dimethylimidazolium complex. The optimized geometries and the related interaction energies (E_{int}, the CCSD(T) level total interaction energy at the basis set limit) are shown in Figure 4. Both structures are T-

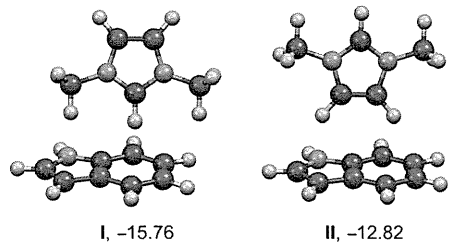

Figure 4. Optimized geometries and CCSD(T) interaction energies at the basis set limit (kcal mol^{-1}) for an indole/1,3-dimethylimidazolium complex.

shaped. Structure **I** (−15.76 kcal mol^{-1}) in which the C_2–H bond of imidazolium points toward the center of six-membered ring of indole is more stable than **II** (−12.82 kcal mol^{-1}) in which the C4–H and C5–H bonds of the imidazolium ion have contact with the indole. The larger electrostatic and induction interactions in **I** compared with **II** (Table 4) are the origin of the greater stability of the geometry **I**. The center of the positive charge distributions of imidazolium ring is close to the midpoint between the two nitrogen atoms of the imidazolium ring.[26] The shorter distance between the midpoint and the indole plane in geometry **I** is apparently the cause of the larger electrostatic and induction energies.

Calculated interaction energies for the complex are compared with those for the benzene complexes with pyridinium and K^+ cations in Table 4. The E_{int} for the most stable form (**I**) is larger than that of the benzene/pyridinium complex (−14.77 kcal mol^{-1}) and also close to that of the benzene/K^+ complex (−17.2 kcal mol^{-1}), which indicates that strong attraction that exists between an indole and a 1,3-di-

Table 4. Electrostatic, induction, and dispersion energies of indole/1,3-dimethylimidazolium and other cation/π complexes.[a]

	E_{HF}[b]	E_{int}[c]	E_{es}[d]	E_{ind}[e]	E_{shot}[f]	E_{corr}[g]
I	−8.70	−15.76	−8.86	−6.57	6.73	−7.06
II	−5.82	−12.82	−7.45	−5.19	6.82	−7.01
benzene/piridinium[h]		−14.77	−8.12	−9.13	8.12	−5.63
benzene/K^+[h]		−17.2	−11.9	−12.8	11.8	−4.4

[a] Energy in kcal mol^{-1}. The geometries of clusters **I** and **II** are shown in Figure 4. [b] HF/aug-cc-pVTZ interaction energy. [c] Estimated CCSD(T) interaction energy at the basis set limit (ECCSD(T) limit). [d] Electrostatic energy. [e] Induction energy. [f] Repulsion energy. [g] Effect of electron correlation on the interaction energy; mainly dispersion energy. [h] Data in ref. [23].

methylimidazolium cation. The large electrostatic and induction contributions to the attraction in the indole/1,3-dimethylimidazolium complex, as in the cases of the benzene complexes with pyridinium and alkali-metal cations, show that the interactions in the indole/1,3-dimethylimidazolium complex should be categorized as a cation–π interaction.

A plausible reaction mechanism is shown in Scheme 5. Although the reaction mechanism through the imidazolium-mediated hydrogen-bonding activation of conjugate acceptors such as Brønsted acid catalysis cannot be excluded,[14,27] based on the results of our mechanistic studies, we propose a catalytic process involving possible cation–π interactions of indole/imidazolium complexes. The cation–π interaction of imidazolium salts with indole leads to the formation of an indole/imidazolium complex (**III**). Close juxtaposition of imidazolium cations to electron-rich indole rings, which leads to the increased acidity of indoles,[28] would facilitate a Lewis base activation of the NH group of the indole by the imidazolium salt-derived chloride anion. This is followed by Friedel–Crafts-type conjugate addition to the acceptor, presumably activated by the hydroxy group of $HyMes^+$, to generate the corresponding enolate **IV**. Subsequent tautomerization of **IV** affords the 3-substituted indole **4a** and regenerates the imidazolium-salt catalyst.

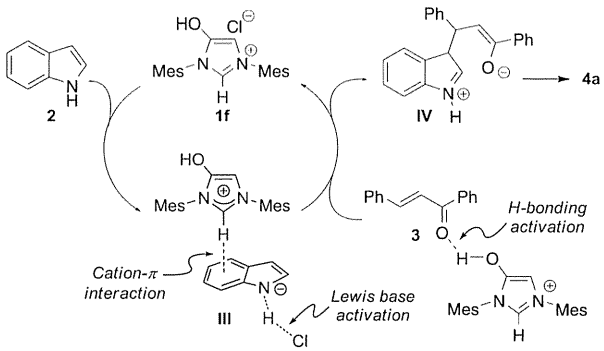

Scheme 5. Proposed reaction mechanism.

Conclusions

We have described an imidazolium salt-catalyzed Friedel–Crafts-type conjugate addition of indoles that requires no base, no solvent, and no carbene to provide various 3-substituted indoles in good to excellent yields at ambient temperatures. The key to this reaction catalyzed by imidazolium salts is the unique activation of indoles prompted by the possible cation/π interaction of indole/imidazolium complexes. High-level ab initio calculation reveals that there is a strong attraction between the indole and the 1,3-dimethylimidazolium cation, and that the most stable T-shaped structure of indole/imidazolium complex is stabilized by large electrostatic and induction interactions, which is a characteristic feature of the cation–π interaction. These findings expand the potential for the development of novel reactions based on these classes of molecules. Efforts to develop an enantioselective version[29] of this reaction and to explore the detailed mechanism are currently in progress.

Experimental Section

General Procedure for Azolium Salt-Catalyzed Friedel–Crafts-Type Conjugate Addition of Indole **2**.

Chalcone **3** (0.50 mmol, 1.0 equiv.), indole (**2**, 2.0 equiv.), and HyMesCl (**1e**, 10 mol%) were placed in a test tube. The reaction mixture was stirred at 40°C for 24 h. Purification by flash column chromatography on silica gel with *n*-hexane/EtOAc gave the corresponding compound **4a**.

Acknowledgements

This research was supported by a Grant-in-Aid for Scientific Research on Innovative Areas "Advanced Molecular Transformations by Organocatalysts" from The Ministry of Education, Culture, Sports, Science and Technology, Japan. We are grateful to Prof. Dr. T. Ohwada (The University of Tokyo) and Prof. Dr. S. Yamada (Ochanomizu University) for helpful discussions.

[1] For reviews, see: a) J. C. Ma, D. A. Dougherty, *Chem. Rev.* **1997**, *97*, 1303; b) J. P. Gallivan, D. A. Dougherty, *Proc. Natl. Acad. Sci. USA* **1999**, *96*, 9459; c) N. Zacharias, D. A. Dougherty, *Trends Pharmacol. Sci.* **2002**, *23*, 281; d) D. A. Dougherty, *Acc. Chem. Res.* **2013**, *46*, 885.

[2] For discussion of cation–π interaction in protein structures, see: a) L. Brocchieri, S. Karlin, *Proc. Natl. Acad. Sci. USA* **1994**, *91*, 9297; b) S. Karlin, M. Zuker, L. Brocchieri, *J. Mol. Biol.* **1994**, *239*, 227.

[3] For reviews, see: a) H.-J. Schneider, *Chem. Soc. Rev.* **1994**, *23*, 227; b) N. S. Scrutton, A. R. Raine, *Biochem. J.* **1996**, *319*, 1; c) E. A. Meyer, R. K. Castellano, F. Diederich, *Angew. Chem. Int. Ed.* **2003**, *42*, 1210; *Angew. Chem.* **2003**, *115*, 1244; d) H.-J. Schneider, *Angew. Chem. Int. Ed.* **2009**, *48*, 3924; *Angew. Chem.* **2009**, *121*, 3982; e) L. M. Salonen, M. Ellermann, F. Diedrich, *Angew. Chem. Int. Ed.* **2011**, *50*, 4808; *Angew. Chem.* **2011**, *123*, 4908.

[4] S. Yamada, C. Morita, *J. Am. Chem. Soc.* **2002**, *124*, 8184.

[5] K. Ishihara, M. Fushimi, *Org. Lett.* **2006**, *8*, 1921.

[6] a) R. R. Knowles, S. Lin, E. N. Jacobsen, *J. Am. Chem. Soc.* **2010**, *132*, 5030; b) C. Uyeda, E. N. Jacobsen, *J. Am. Chem. Soc.* **2011**, *133*, 5062. For a recent review of noncovalent interactions, see:

R. R. Knowles, E. N. Jacobsen, *Proc. Natl. Acad. Sci. USA* **2010**, *107*, 20678.

[7] For examples of organocatalysis involving possible cation–π interactions, see: a) D. L. Comins, S. P. Joseph, R. R. Goehring, *J. Am. Chem. Soc.* **1994**, *116*, 4719; b) T. Kawabata, M. Nagato, K. Takasu, K. Fuji, *J. Am. Chem. Soc.* **1997**, *119*, 3169; c) S. J. Miller, G. T. Copeland, N. Papaioannou, T. E. Horstmann, E. M. Ruel, *J. Am. Chem. Soc.* **1998**, *120*, 1629; d) K. A. Ahrendt, C. J. Borths, D. W. C. MacMillan, *J. Am. Chem. Soc.* **2000**, *122*, 4243; e) V. B. Birman, E. W. Uffman, J. Hui, X. M. Li, C. J. Kilbane, *J. Am. Chem. Soc.* **2004**, *126*, 12226; S. M. Mennen, J. T. Blank, M. B. Tran-Dube, J. E. Imbriglio, S. J. Miller, *Chem. Commun.* **2005**, 195; f) B. Hu, M. Meng, Z. Wang, W. Du, J. S. Fossey, X. Hu, W.-P. Deng, *J. Am. Chem. Soc.* **2010**, *132*, 17041. For a recent review, see: S. Yamada, J. S. Fossey, *Org. Biomol. Chem.* **2011**, *9*, 7257.

[8] For recent reviews of organocatalytic Friedel–Crafts reactions, see: a) V. Terrasson, R. M. de Figueiredo, J. M. Campagne, *Eur. J. Org. Chem.* **2010**, 2635; b) M. Rueping, B. J. Nachtsheim, *Beilstein J. Org. Chem.* **2010**, *6*, 6; c) S.-L. You, Q. Cai, M. Zeng, *Chem. Soc. Rev.* **2009**, *38*, 2190.

[9] For reviews, see: a) J. M. Moore, T. Rovis in *Topics in Current Chemistry, Vol. 291* (Ed.: B. List), Springer, Berlin, **2009**, pp. 77–144; b) D. Enders, O. Niemeier, A. Henseler, *Chem. Rev.* **2007**, *107*, 5606; c) K. Zeitler, *Angew. Chem. Int. Ed.* **2005**, *44*, 7506; *Angew. Chem.* **2005**, *117*, 7674; d) D. Enders, T. Balensiefer, *Acc. Chem. Res.* **2004**, *37*, 534; e) P.-C. Chiang, J. W. Bode in *N-Heterocyclic Carbenes: From Laboratory Curiosities to Efficient Synthetic Tools* (Ed.: S. Díes-Conzález), Royal Society of Chemistry, Cambridge, **2010**, pp. 399–435.

[10] M. Movassaghi, M. A. Schmidt, *Org. Lett.* **2005**, *7*, 2453.

[11] E. M. Phillips, M. Riedrich, K. A. Scheidt, *J. Am. Chem. Soc.* **2010**, *132*, 13179.

[12] Q. Kang, Y. Zhang, *Org. Biomol. Chem.* **2011**, *9*, 6715.

[13] See the Supporting Information for details.

[14] For a similar reaction of thiols with enones catalyzed by an ionic liquid via hydrogen-bonding interactions with the C2 hydrogen atom of imidazolium ions, see: A. Sarkar, S. R. Roy, A. K. Chakraborti, *Chem. Commun.* **2011**, *47*, 4538. For several transformations mediated by azolium ions as acid catalysts, see: a) V. Jurcík, R. Wilhelm, *Tetrahedron: Asymmetry* **2006**, *17*, 801; b) A. K. Chakraborti, S. R. Roy, *J. Am. Chem. Soc.* **2009**, *131*, 6902; c) P. V. G. Reddy, S. Tabassum, A. Blanrue, R. Wilhelm, *Chem. Commun.* **2009**, *45*, 5910; d) S. R. Roy, A. K. Chakraborti, *Org. Lett.* **2010**, *12*, 3866; e) L. Myles, R. Gore, M. Špulák, N. Gathergood, S. J. Connon, *Green Chem.* **2010**, *12*, 1157; f) A. Sarkar, S. R. Roy, N. Parikh, A. K. Chakraborti, *J. Org. Chem.* **2011**, *76*, 7132; g) L. Myles, N. Gathergood, S. J. Connon, *Chem. Commun.* **2013**, *49*, 5316.

[15] a) J. Kaeobamrung, J. Mahatthananchai, P. Zheng, J. W. Bode, *J. Am. Chem. Soc.* **2010**, *132*, 8810; b) J. Mahatthananchai, J. Kaeobamrung, J. W. Bode, *ACS Catal.* **2012**, *2*, 494.

[16] For the synthesis of HyMesCl **1f**, see: a) L. Benhamou, V. César, H. Gornitzka, N. Lugan, G. Lavigne, *Chem. Commun.* **2009**, 4720; b) L. Benhamou, N. Vujkovic, V. César, H. Gornitzka, N. Lugan, G. Lavigne, *Organometallics* **2010**, *29*, 2616.

[17] For recent reviews on chiral phosphoric acid catalysts, see: a) S. J. Connon, *Angew. Chem. Int. Ed.* **2006**, *45*, 3909; *Angew. Chem.* **2006**, *118*, 4013; b) T. Akiyama, J. Itoh, K. Fuchibe, *Adv. Synth. Catal.* **2006**, *348*, 999; c) T. Akiyama, *Chem. Rev.* **2007**, *107*, 5744; d) G. Adair, S. Mukherjee, B. List, *Aldrichimica Acta* **2008**, *41*, 31; e) M. Terada, *Chem. Commun.* **2008**, 4097; f) M. Terada, *Bull. Chem. Soc. Jpn.* **2010**, *83*, 101; g) M. Terada, *Synthesis* **2010**, 1929; h) A. Zamfir, S. Schenker, M. Freund, S. B. Tsogoeva, *Org. Biomol. Chem.* **2010**, *8*, 5262; i) M. Terada, *Curr. Org. Chem.* **2011**, *15*, 2227.

[18] T. Sakamoto, J. Itoh, K. Mori, T. Akiyama, *Org. Biomol. Chem.* **2010**, *8*, 5448.

[19] F. G. Bordwell, G. E. Drucker, H. E. Fried, *J. Org. Chem.* **1981**, *46*, 632.

[20] a) E. Alcalde, C. Alvarez-Rua, S. García-Granda, E. García-Rodriguez, N. Mesquida, L. Pérez-García, *Chem. Commun.* **1999**, 295; b) E. Alcalde, N. Mesquida, L. Pérez-García, *Eur. J. Org. Chem.* **2006**, 3988; c) I. Dinarès, C. G. de Miguel, N. Masquida, E. Aldalde, *J. Org. Chem.* **2009**, *74*, 482.

[21] Gaussian 09, Revision C.01, M. J. Frisch, et al. Gaussian, Inc., Wallingford CT, **2009**.

[22] a) M. Head-Gordon, J. A. Pople, M. J. Frisch, *Chem. Phys. Lett.* **1988**, *153*, 503; b) J. A. Pople, M. Head-Gordon, K. Raghavachari, *J. Chem. Phys.* **1987**, *87*, 5968; c) B. J. Ransil, *J. Chem. Phys.* **1961**, *34*, 2109; d) S. F. Boys, F. Bernardi, *Mol. Phys.* **1970**, *19*, 553; e) T. Helgaker, W. Klopper, H. Koch, J. Noga, *J. Chem. Phys.* **1997**, *106*, 9639; f) S. Tsuzuki, K. Honda, T. Uchimaru, M. Mikami, K. Tanabe, *J. Am. Chem. Soc.* **2000**, *122*, 3746; g) K. Shibasaki, A. Fujii, M. Mikami, S. Tsuzuki, *J. Phys. Chem. A* **2007**, *111*, 753; h) A. J. Stone, M. Alderton, *Mol. Phys.* **1985**, *56*, 1047; i) A. J. Stone, *The theory of intermolecular forces*, Clarendon Press, Oxford, **1996**; j) A. J. Stone, A. Dullweber, M. P. Hodges, P. L. A. Popelier, D. J. Wales, *Orient: a program for studying interactions between molecules version 3.2*. University of Cambridge, **1995**; k) A. J. Stone, *J. Chem. Theory Comput.* **2005**, *1*, 1128–1132; l) A. J. Stone, *Mol. Phys.* **1985**, *56*, 1065; m) P. T. van Duijnen, M. Swart, *J. Phys. Chem. A* **1998**, *102*, 2399.

[23] a) T. H. Dunning, Jr., *J. Phys. Chem. A* **2000**, *104*, 9062; b) S. Tsuzuki, T. Uchimaru, K. Matsumura, M. Mikami, K. Tanabe, *J. Chem. Phys.* **1999**, *110*, 11906.

[24] S. Tsuzuki, M. Mikami, S. Yamada, *J. Am. Chem. Soc.* **2007**, *129*, 8656, and references therein.

[25] S. Mecozzi, A. P. West, D. A. Dougherty, *Proc. Natl. Acad. Sci. USA* **1996**, *93*, 10566.

[26] S. Tsuzuki, H. Tokuda, M. Mikami, *Phys. Chem. Chem. Phys.* **2007**, *9*, 4780.

[27] It should be note that although an alternative mechanism catalyzed by the Brønsted acid catalysts **V** and **VI** that might be generated from the Mannich-type reaction of indole to imidazolium would be possible, neither **V** nor **VI** were detected by ^{1}H NMR spectroscopy. For a discussion of imidazolium-derived ionic liquids as Brønsted acid catalysts in the presence of protic additives, such as alcohols, see ref. 14e.

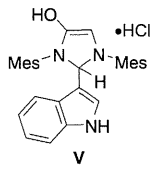

V

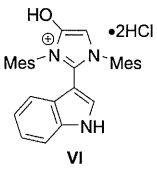

VI

[28] Atomic charge distributions of indole were calculated by electrostatic potential fitting using Merz-Singh-Kollman Scheme from the MP2/6-311G** wavefunctions of isolated indole and an indole-dimethylimidazolium complex, indicating that a cation–π interaction in the indole/imidazolium complex largely affect the atomic charge distributions of indole, rendering the NH group of indole more cationic. See the Supporting Information for details.

[29] Several chiral imidazolium salts with a hydroxy group for the enantioselective reaction were attempted, but no enantioselectivity was achieved. See the Supporting Information for details.

Received: January 30, 2014
Published online: March 24, 2014

Organic LETTERS

Letter

pubs.acs.org/OrgLett

Isostere-Based Design of 8-Azacoumarin-Type Photolabile Protecting Groups: A Hydrophilicity-Increasing Strategy for Coumarin-4-ylmethyls

Tetsuo Narumi,[†,§,#] Hikaru Takano,[†,#] Nami Ohashi,[†] Akinobu Suzuki,[‡] Toshiaki Furuta,[‡] and Hirokazu Tamamura*[,†]

[†]Institute of Biomaterials and Bioengineering, Tokyo Medical and Dental University, Chiyoda-ku, Tokyo 101-0062, Japan

[‡]Department of Biomolecular Science, Toho University, 2-2-1 Miyama, Funabashi, Chiba 274-8510, Japan

Supporting Information

ABSTRACT: Described is the development of 8-azacoumarin-4-ylmethyl groups as aqueous photolabile protecting groups. A key feature of the strategy is the isosteric replacement of the C7–C8 enol double bond of the Bhc derivative with an amide bond, resulting in conversion of the chromophore from coumarin to 8-azacoumarin. This strategy makes dramatically enhanced water solubility and facile photocleavage possible.

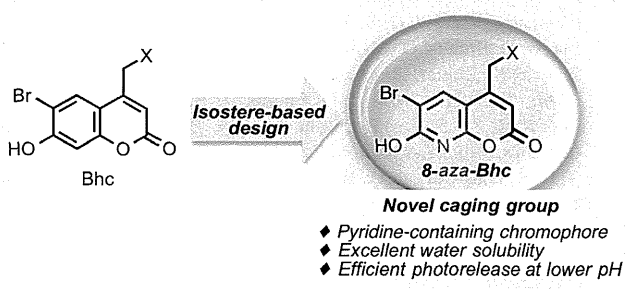

Chemical processes mediated by photolabile protecting groups find numerous utilities in synthetic organic chemistry,[1] chemical biology, and cell biology.[2] The exceptional utilities of photolabile protecting groups include their mild conditions associated with the photocleavage that can proceed smoothly and quickly even in aqueous conditions and their potential as photoactivatable molecules or caged compounds that enable spatial and temporal control of their biological functions.[3] Among various caging groups,[4−7] coumarins have had widespread applications to caging chemistry in recent years. In particular, the potential of two-photon photolysis with practically useful absorption cross sections (720–900 nm) is among the outstanding advantages of coumarin types such as the 6-bromo-7-hydroxycoumarin-4-ylmethyl (Bhc) group.[7d] However, one of the drawbacks of coumarin types is their low aqueous solubility. Aqueous solubility is critical for the utility of caged compounds, since hydrophobic caged compounds will be aggregated in physiological conditions and the photocleavage would be plagued by sluggish reactivity.[7h]

There are a few methods for increasing the aqueous solubility of coumarin chromophores. One successful example is the introduction of one or more hydrophilic carboxyl groups such as BCMACM,[8] BBHCM,[9] and DEAC450.[10] Although these approaches effectively achieve the increase of hydrophilicity of coumarin chromophores, the development of new strategies for increasing the hydrophilicity with high photosensitivity remains challenging.

In this report, we disclose a simple and powerful strategy based on the concept of the amide-alkene isosterism for increasing the hydrophilicity of coumarin-type photolabile protecting groups (Figure 1), leading to the development of novel 8-azacoumarin-type protecting groups. The newly designed 8-azacoumarin-type protecting groups have approximately 10- to 18-fold enhanced solubility in aqueous buffer compared to that of the parent Bhc group and possess photophysical and photochemical properties favorable for caging chemistry. Our presented strategy has the potential to provide new solutions for the development of caged compounds with enhanced hydrophilicity.

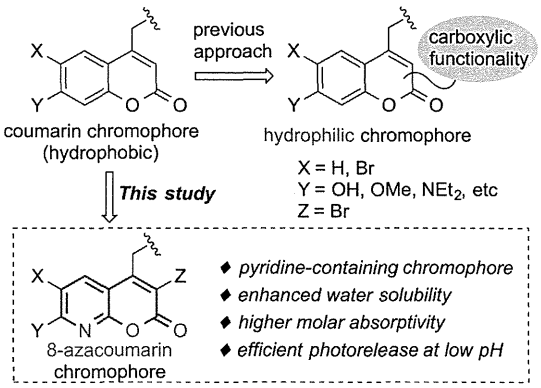

Figure 1. Strategies to increase the hydrophilicity of the coumarin chromophore.

Our studies started from the design of novel chromophores with enhanced hydrophilicity (Figure 2). Our approach to increasing hydrophilicity is based on the introduction of polar and hydrophilic amide functionality into the coumarin chromophore. As shown in Figure 2, the C7–C8 enol double

Received: January 7, 2014
Published: February 4, 2014

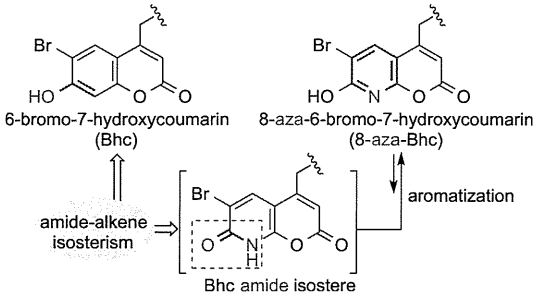

Figure 2. Isostere-based design of an 8-azacoumarin-type photolabile protecting group.

bond of the coumarin chromophore was replaced with an amide bond followed by aromatization of the lactam moiety to form a hydroxypyridine-containing 8-azacoumarin chromophore. This strategy relies on the concept of structural isosterism of amides and alkenes (enols), familiar in medicinal chemistry[11] and exemplified by alkene-type dipeptide isosteres,[12] which are regarded as ideal ground state mimetics of dipeptides and thus have been applied to many biologically active peptides.[13]

Our synthesis of 8-azacoumarins with a hydroxylmethyl group at the C4 position began with 2,6-dichloropyridine **3** (Scheme 1). Successive treatments of **3** with potassium *tert*-

Scheme 1. Synthesis of Azacoumarin Derivatives 7 and 9

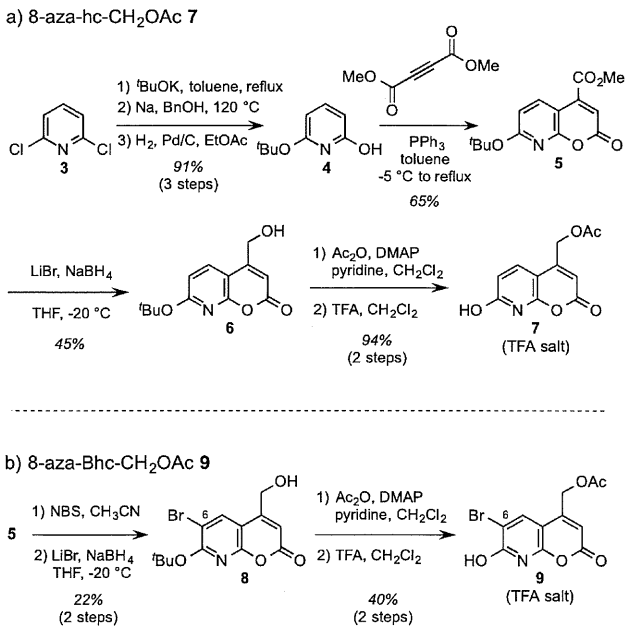

butoxide and sodium benzyl alkoxide followed by hydrogenolysis of the benzyl group afforded the hydroxypyridine derivative **4** in an excellent yield (91% in 3 steps). Reaction of **4** with dimethyl acetylenedicarboxylate (DMAD) in the presence of PPh_3 provided the desired 8-azacoumarin **5** with an ester functionality at the C4 position in 65% yield.[14] Chemoselective reduction was required for the conversion of this conjugated ester of **5** to the corresponding alcohol, since the lactone moiety of 8-azacoumarin is subject to cleavage by reducing agents. Screening of various reducing agents revealed that the use of $LiBH_4$ prepared *in situ* in THF at −20 °C afforded acceptable conversion giving the desired 8-azacoumarin derivative **6** with a hydroxylmethyl group at the C4 position, in 45% isolated yield. Compound **6** was subjected to acetylation of the alcohol followed by TFA treatment to give the desired 4-acetoxymethyl-8-aza-hc (8-aza-hc-CH_2OAc, **7**). Furthermore, in order to study the substituent (heavy atom) effects[7d] on the 8-azacoumarin chromophore, the 6-brominated derivative (8-aza-Bhc-CH_2OAc, **9**) was also synthesized in a similar manner (Scheme 1b).

The key underlying concept of our approach is the introduction of an amide functionality to the coumarin chromophore to increase the aqueous solubility. The aqueous solubility of 8-azacoumarin derivatives **7** and **9** in PBS (0.1% DMSO) was evaluated with the parent Bhc derivative **10** (Table 1). As expected, 8-azacoumarin derivatives showed

Table 1. Hydrophilic Properties of 8-Azacoumarins 7 and 9 and Bhc Derivative 10

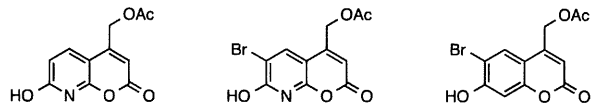

compd	C_s[a] (μM)	pK_a[b]
7	6611	5.67
9	10832	4.22
10	602	5.88[c]

[a]Concentration at saturation in PBS buffer (0.1% DMSO). [b]Determined using citric/phosphate buffer in the pH range 2.6–7.0. [c]Literature value = 6.2 in H_2O.[15]

hydrophilicity much higher than that of **10**; in particular, the saturated concentration (C_s) of 8-aza-Bhc-CH_2OAc **9** was approximately 18-fold greater than that of **10**. These results indicate that the replacement of the chromophore involving the conversion of the coumarin into 8-azacoumarin enabled the enhancement of hydrophilicity of the coumarin chromophore. It is noteworthy that 8-aza-Bhc-CH_2OAc **9** showed hydrophilicity higher than that of the nonbrominated compound **7** possibly due to the lower pK_a value (4.22) of the chromophore. In addition, HPLC monitoring of **9** in PBS at room temperature showed that **9** was highly resistant to spontaneous hydrolysis in the dark and that only 2% of **9** was hydrolyzed in 12 h.[16]

The photochemical properties of azacoumarin derivatives **7**, **9**, and **10** in aqueous solutions were examined. 8-Aza-hc-CH_2OAc **7** was subjected to photolysis in 5 μM KMOPS buffer (10 mM MOPS; 4-morpholinepropane-1-sulfonic acid, and 100 mM KCl) solution at pH 7.2 at 350 nm. Figure 3 shows the time courses of photolysis reactions of synthetic compounds in terms of the consumption of the starting materials and indicates that the photolytic reaction of **7** follows a single-exponential decay with the time to reach 50% conversion (t_{50}) for photolysis of **7** at 29 s. As expected, introduction of the bromo group resulted in the remarkable increase of the photochemical reactivity; the value of t_{50} for photolysis of **9** is 13 s, which is slightly longer than that of **10** (9 s) but is about 2.3 times shorter than that of **7**. Although the photolytic mechanism of 8-azacoumarin derivatives **7** and **9** is not fully understood at this stage, these observations suggest the possibility of 8-azacoumarin-based chromophores working as photolabile protecting groups.

dx.doi.org/10.1021/ol5000583 | *Org. Lett.* 2014, 16, 1184–1187

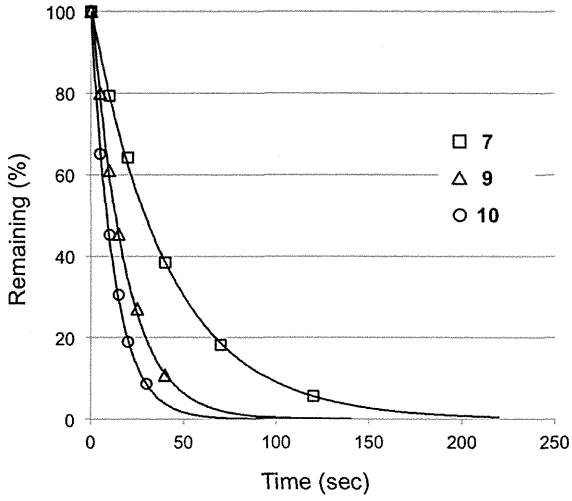

Figure 3. Time courses of photolysis reactions of **7**, **9**, and **10**. Samples were subjected to photolysis in 5 μM KMOPS buffer solution at pH 7.2 at 350 nm (10 mJ/s). All data are the mean values for at least two independent experiments.

Photophysical and photochemical properties of the 8-azacoumarin derivatives **7** and **9** and the Bhc derivative **10** are shown in Table 2. The absorption maxima shifted slightly to shorter wavelength, from 370 nm for **10** to 356 and 362 nm for **7** and **9**, respectively, indicating that like the Bhc group azacoumarin-based protecting groups can be cleaved under uncaging light conditions (330–385 nm). The molar absorptivities at 350 nm of **7** (ε = 20175 M^{-1} cm^{-1}) and **9** (ε = 20583 M^{-1} cm^{-1}) are higher than that of **10**. The photolysis quantum yields for disappearance of starting materials were calculated from the single decay curves using the equation $\Phi = 1/(I \times 10^3 \varepsilon t_{90})$ as reported by Tsien.[17] The quantum yields of disappearance were determined as 0.026 for **7** and 0.059 for **9**, respectively, which are 2–5 times lower than that of **10** (0.13) possibly due to the relatively strong fluorescence of the 8-azacoumarin chromophore.[18] An important factor in the development of new photolabile protecting groups is photolysis efficiency. The photolysis efficiency of caged compounds is evaluated with the product of the photolysis quantum yield (Φ_{chem}) and molar absorptivity (ε) and allows quantitative comparison of the overall efficiency of a photolysis reaction.[19] The $\varepsilon_{350}\cdot\Phi_{chem}$ values of **7** and **9** are 526 and 1211, respectively, and that of **10** is 1806. The observed $\varepsilon_{350}\cdot\Phi_{chem}$ values of 8-azacoumarin derivatives **7** and **9** were sufficiently high to support practical applications to caging chemistry. Taking into account the excellent aqueous solubility of the 8-azacoumarin chromophore, 8-azacoumarin-based photolabile protecting groups promise to be useful for caging chemistry.

Table 2. Selected Photophysical and Photochemical Properties of Compounds 7, 9, and 10

compd	λ_{max} [a] (nm)	ε_{max} [b] (M^{-1} cm^{-1})	ε_{350} [c] (M^{-1} cm^{-1})	Φ_{chem} [d]	$\varepsilon_{350}\cdot\Phi_{chem}$ [e]
7	356	20799	20175	0.026	526
9	362	23520	20583	0.059	1211
10	370	18071	13774	0.13	1806

[a]Long-wavelength absorption maxima. [b]Molar absorptivity at the absorption maxima. [c]Molar absorptivity at 350 nm. [d]Quantum yields for the disappearance of starting materials upon irradiation at 350 nm. [e]Product of the photolysis quantum yield and molar absorptivity.

In conclusion, we have designed and performed a simple and robust strategy for increasing the hydrophilicity of coumarin chromophores based on the concept of structural isosterism of amides and enols. Replacement of the C7–C8 enol double bond of the Bhc group with a polar and hydrophilic amide bond led to the development of novel 8-azacoumarin-type protecting groups, which can be removed photolytically and which showed markedly enhanced hydrophilicity and high photolysis efficiency supporting applications to caging chemistry. These studies provide the basis for future work including the development of novel hydrophilic molecules, to which it is difficult by standard approaches to introduce additional hydrophilic functionalities. Current efforts are aimed at expanding this strategy to other caging groups and functional molecules, which will offer highly effective methods for spatial and temporal control of biological activities.

■ ASSOCIATED CONTENT

Supporting Information

Experimental detail, synthesis, and characterization data. This material is available free of charge via the Internet at http://pubs.acs.org.

■ AUTHOR INFORMATION

Corresponding Author

*E-mail: tamamura.mr@tmd.ac.jp.

Present Address

[§]Department of Applied Chemistry and Biochemical Engineering, Faculty of Engineering, Shizuoka University, Hamamatsu, Shizuoka 432-8561, Japan.

Author Contributions

[#]T.N and H.T. contributed equally to this work.

Notes

The authors declare no competing financial interest.

■ ACKNOWLEDGMENTS

This research was supported by the Naito Foundation (Natural Science Scholarship) and in part by a Grant-in-Aid for Young Scientist (B) from the Ministry of Education, Culture, Sports, Science and Technology. We are grateful to Dr. Tomoya Hirano (Tokyo Medical and Dental University: TMDU) for assistance in the measurement of photophysical properties and to Chiaki Kambe (TMDU) for preliminary experiments.

■ REFERENCES

(1) (a) Pillai, V. N. R. *Synthesis* **1980**, 1–26. (b) Binkley, R. W.; Flechtner, T. W. In *Synthetic Organic Photochemistry*; Horspool, W. M., Ed.; Plenum: New York, 1984; pp 375–423. (c) Pillai, V. N. R. *Organic Photochemistry*; Padwa, A., Ed.; Marcel Dekker: New York, 1987; Vol. 9, pp 225–323. (d) Bochet, C. G. *J. Chem. Soc., Perkin Trans. 1* **2002**, 125–142. (e) Bochet, C. G.; Blanc, A. In *CRC Handbook of Organic Photochemistry and Photobiology*; Griesbeck, A., Oelgemöller, M., Ghetti, F., Eds.; CRC: Boca Raton, 2012; Vol. 1, pp 73–93. (f) Klán, P.; Šolomek, T.; Bochet, C. G.; Blanc, A.; Givens, R.; Rubina, M.; Popik, V.; Kostikov, A.; Wirz, J. *Chem. Rev.* **2013**, *113*, 119–191.

(2) (a) Adams, S. R.; Tsien, R. Y. *Annu. Rev. Physiol.* **1993**, *55*, 755–784. (b) Curley, K.; Lawrence, D. S. *Pharmacol. Ther.* **1999**, *82*, 347–354. (c) Dorman, G.; Prestwich, G. D. *Trends Biotechnol.* **2000**, *18*,

64–77. (d) Shigeri, Y.; Tatsu, Y.; Yumoto, N. *Pharmacol. Ther.* **2001**, *91*, 85–92.
(3) (a) Caged Compounds. In *Methods in Enzymology*; Marriot, G., Ed.; Academic Press: New York, 1998; Vol. *291*. (b) Mayer, G.; Heckel, A. *Angew. Chem., Int. Ed.* **2006**, *45*, 4900–4921. (c) Ellis-Davies, G. C. R. *Nat. Methods* **2007**, *4*, 619–628. (d) Lee, H. M.; Larson, D. R.; Lawrence, D. S. *ACS Chem. Biol.* **2009**, *4*, 409–427.
(4) Nitrobenzyl-type: (a) Engels, J.; Schlaeger, E.-J. *J. Med. Chem.* **1977**, *20*, 907–911. (b) Kaplan, J. H.; Forbush, B., III; Hoffman, J. F. *Biochemistry* **1978**, *17*, 1929–1935.
(5) Benzoin-type: (a) Sheehan, J. C.; Wilson, R. M. *J. Am. Chem. Soc.* **1964**, *86*, 5277–5281. (b) Givens, R. S.; Athey, P. S.; Kueper, L. W., III; Matuszewski, B.; Xue, J. *J. Am. Chem. Soc.* **1992**, *114*, 8708–8710. (c) Hansen, K. C.; Rock, R. S.; Larsen, R. W.; Chan, S. I. *J. Am. Chem. Soc.* **2000**, *122*, 11567–11568.
(6) Phenacyl-type: (a) Sheehan, J. C.; Umezawa, K. *J. Org. Chem.* **1973**, *38*, 3771–3774. (b) Givens, R. S.; Weber, J. F. W.; Jung, A. H.; Park, C.-H. *Methods Enzymol.* **1998**, *291*, 1–29. (c) Conrad, P. G., II; Givens, R. S.; Weber, J. F. W.; Kandler, K. *Org. Lett.* **2000**, *2*, 1545–1547.
(7) Coumarin-type: (a) Givens, R. S.; Matuszewski, B. *J. Am. Chem. Soc.* **1984**, *106*, 6860–6861. (b) Furuta, T.; Torigai, H.; Sugimoto, M.; Iwamura, M. *J. Org. Chem.* **1995**, *60*, 3953–3956. (c) Furuta, T.; Iwamura, M. *Methods Enzymol.* **1998**, *291*, 50–63. (d) Furuta, T.; Wang, S. S. H.; Dantzker, J. L.; Dore, T. M.; Bybee, W. J.; Callaway, E. M.; Denk, W.; Tsien, R. Y. *Proc. Natl. Acad. Sci. U.S.A.* **1999**, *96*, 1193–1200. (e) Hagen, V.; Bendig, J.; Fring, S.; Eckardt, T.; Helm, S.; Reuter, D.; Kaupp, U. B. *Angew. Chem., Int. Ed.* **2001**, *40*, 1045–1048. (f) Eckardt, T.; Hagen, V.; Schade, B.; Schmidt, R.; Schweitzer, C.; Bendig, J. *J. Org. Chem.* **2002**, *67*, 703–710. (g) Geisler, D.; Kresse, W.; Wiesner, B.; Bendig, J.; Kettenmann, H.; Hagen, V. *ChemBioChem* **2003**, *4*, 162–170. (h) Nomura, W.; Narumi, T.; Ohashi, N.; Serizawa, Y.; Lewin, N. E.; Blumberg, P. M.; Furuta, T.; Tamamura, H. *ChemBioChem* **2011**, *12*, 535–539.
(8) Hagen, V.; Dekowski, B.; Nache, V.; Schmidt, R.; Geissler, D.; Lorenz, D.; Eichhorst, J.; Keller, S.; Kaneko, H.; Benndorf, K.; Wiesner, B. *Angew. Chem., Int. Ed.* **2005**, *44*, 7887–7891.
(9) Hagen, V.; Kilic, F.; Schaal, J.; Dekowski, B.; Schmidt, V. R.; Kotzur, N. *J. Org. Chem.* **2010**, *75*, 2790–2797.
(10) Olson, J. P.; Kwon, H.-B.; Takasaki, K. T.; Chiu, C. Q.; Higley, M. J.; Sabatini, B. L.; Ellis-Davies, G. C. R. *J. Am. Chem. Soc.* **2013**, *135*, 5954–5957.
(11) (a) Kim, B. H.; Venkatsean, N. *Curr. Med Chem.* **2002**, *9*, 2243–2270. (b) Meanwell, N. A. *J. Med. Chem.* **2011**, *54*, 2529–2591.
(12) For some examples of unsubstituted alkene dipeptide isosteres, see: (a) Jenkins, C. L.; Vasbinder, M. M.; Miller, S. J.; Raines, R. T. *Org. Lett.* **2005**, *7*, 2619–2622. (d) Wiktelius, D.; Luthman, K. *Org. Biomol. Chem.* **2007**, *5*, 603–605. (e) Badur, N. G.; Harms, K.; Koert, U. *Synlett* **2007**, *1*, 99–102 and references therein.
(13) (a) Namanja, A.; Wang, X. J.; Xu, B.; Mercedes-Camacho, A. Y.; Wilson, B. D.; Wilson, K. A.; Etzkorn, F. A.; Peng, J. W. *J. Am. Chem. Soc.* **2010**, *132*, 5607–5609. (b) Tamamura, H.; Hiramatsu, K.; Ueda, S.; Wang, Z.; Kusano, S.; Terakubo, S.; Trent, J. O.; Peiper, S. C.; Yamamoto, N.; Nakashima, H.; Otaka, A.; Fujii, N. *J. Med. Chem.* **2005**, *48*, 380–391. (c) Narumi, T.; Hayashi, R.; Tomita, K.; Kobayashi, K.; Tanahara, N.; Ohno, H.; Naio, T.; Kodama, E.; Matsuoka, M.; Oishi, S.; Fujii, N. *Org. Biomol. Chem.* **2010**, *8*, 616–621 and references therein.
(14) Yavari, I.; Adib, M.; Hojabri, L. *Tetrahedron* **2002**, *58*, 6895–6899.
(15) Furuta, T.; Takeuchi, H.; Isozaki, M.; Takahashi, Y.; Kanehara, M.; Sugimoto, M.; Watanabe, T.; Noguchi, K.; Dore, T. M.; Kurahashi, T.; Iwamura, M.; Tsien, R. Y. *ChemBioChem* **2004**, *5*, 1119–1128.
(16) HPLC monitoring of the hydrolysis stability in PBS of azacoumarins revealed that compound **7** was more resistant than the parent Bhc **10**. See Supporting Information for details.
(17) Tsien, R. Y.; Zuker, R. S. *Biophys. J.* **1986**, *50*, 843–853.
(18) The quantum yields of fluorescence were determined as 0.39 for **7** and 0.29 for **9**, respectively.
(19) Brown, E. B.; Shear, J. B.; Adams, S. R.; Tsien, R. Y.; Webb, W. W. *Biophys. J.* **1999**, *76*, 489–499.

dx.doi.org/10.1021/ol5000583 | *Org. Lett.* 2014, 16, 1184–1187

ターゲットタンパク質を特異的に認識するプローブ

野村 渉[*1]・玉村啓和[*2]

1．タグ-プローブシステム

タンパク質は物質の変換・輸送・情報伝達などの機能を司っている重要な生体高分子であり，生命現象をより深く理解するためには，生きた細胞におけるタンパク質の機能や局在，タンパク質間の相互作用について詳細に解析することが不可欠である．現在ではさまざまな蛍光分子を用いて生細胞内外のタンパク質を可視化できる手法が開発されている．最も広く用いられているタンパク質の蛍光ラベル化は，1960年代下村らにより発見されたGreen Fluorescent Protein (GFP)を蛍光タンパク質として融合する方法である[1]．GFPを用いる可視化は非常に有用な方法であり，蛍光イメージングにおいて大きく貢献し，GFPを改変したさまざまな色の蛍光タンパク質を用いた蛍光ラベル化が可能になっている．近年では，時間依存的に発現動態や局在，活性化・不活性化状態が大きく変化するタンパク質についてより詳細に解析することに焦点が当てられ，標的タンパク質を特定の時間に観測する手法の開発が求められている．そこで，標的タンパク質にタグとなるタンパク質またはペプチドを付加し，そのタグと特異的に結合する蛍光プローブを後から加えて蛍光ラベル化を達成するタグ-プローブシステムが有用なイメージングツールとして期待されている．われわれのペプチドタグ-プローブペアを開発する以前までのそれらの例としては，テトラシステインタグ(-Cys-Cys-X-X-Cys-Cys-)と2個の砒素原子を有する蛍光プローブ(FlAsH等)の組み合わせ[2]や，酵素自体をタグとし基質の蛍光誘導体をプローブとして利用したHaloタグ[3]，金属錯体とそのリガンドとの間の強い親和性を利用したD4タグ(Asp4残基を含む)-二核亜鉛錯体プローブ[4]等があった．ほとんどのタグ-プローブペアにおいて，タグに結合していない遊離のプローブ分子由来の蛍光がバックグラウンドとして観測されてしまうなどの問題点があげられていた．

2．ZIPタグ-プローブペア

これまでに報告されているロイシンジッパー構造[5]に着目し，すでに結晶構造が明らかにされている逆平行3本鎖ペプチド[6]を基本骨格としたタグ-プローブペア(ZIPタグ-プローブペア)を開発した．3本鎖のうち1本鎖をプローブペプチド，2本鎖をタグペプチドとした．プローブペプチドには，環境応答性色素として4-nitrobenzo-2-oxa-1,3-diazole (NBD)を導入したNBDプローブ分子を設計，合成した．そして，ロイシンジッパー構造内部(3本鎖の内側)に形成される疎水性ポケットのサイズを最適化するため，タグ配列のポケット形成に関わる2個のロイシンをアラニ

*1 Wataru Nomura 東京医科歯科大学生体材料工学研究所 准教授 博士(薬学)
*2 Hirokazu Tamamura 同上 教授 博士(薬学)
Specific Probes Recognizing Target Proteins

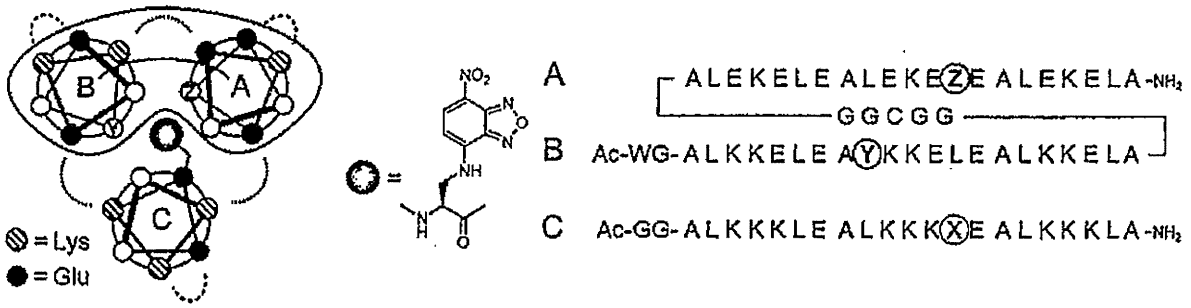

図1　ZIPタグ-プローブペアのデザイン．二本鎖ペプチドAとBをGGCGGリンカーでつないで，タグペプチドとした．一本鎖ペプチドCにX(NBDを導入した2,3-diaminopropionic acid)を導入し，プローブペプチドとした．YとZはもとのLeuをAlaに置換した

ンに置換したタグペプチドを設計，合成した(図1)．これらのタグとNBDプローブペアについてHEPES buffer中にて蛍光滴定実験を行い，タグ-NBDプローブペアの結合親和性および蛍光応答能の評価を行うと，結合に伴う約18倍の蛍光強度の増加と30 nmの蛍光波長の短波長シフトが見られた(図2)．NBDプローブ単独では微弱な黄色の蛍光しか示さないのに対し，タグ-NBDプローブペアの溶液では明るい緑色の蛍光が観測され，これらの差は肉眼でも識別可能である．タグ-NBDプローブペアの解離定数は17.5 nMであり，抗原-抗体並みの結合親和性を有している．また，タグとの結合に伴ってNBDプローブの蛍光強度と蛍光波長が大幅に変化するため，遊離のプローブと容易に区別して標的タンパク質の蛍光イメージングが可能となる．これはタンパク質の蛍光イメージングに用いるには十分な親和性であるといえる．さらに，円二色性スペクトルよりNBDプローブペプチドとタグペプチドが安定な三本鎖α-ヘリックス構造を形成していることを確認している[7]．

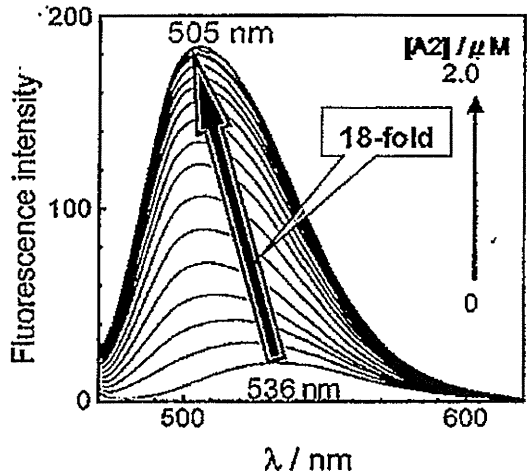

図2　ZIPタグ-NBDプローブペアの蛍光滴定

3．ZIPタグ-プローブシステムによる細胞表面タンパク質のイメージング

このZIPタグ-プローブシステムが生細胞においても同様に機能するかどうか検討するため，タグ-NBDプローブペアを用いて細胞表面に存在する膜タンパク質であるケモカイン受容体CXCR4の蛍光イメージングを実施した(図3)．その結果，洗浄操作無しでもCXCR4を蛍光ラベル化して観察することに成功した．また，本現象はCXCR4アンタゴニストのtetramethylrhodamine(TAMRA)標識体[8]を用いるダブルラベリングにより証明している．

4．ZIPタグ-プローブシステムによる細胞内タンパク質のイメージング

次に，ZIPタグ-プローブシステムが細胞内のタンパク質に対しても同様に機能するかどうか検討するため，細胞内に存在するタンパク質リン酸化酵素PKCの蛍光イメージングを実施した(図4)．まず，NBDプローブのC末に細胞膜透過シグナルであるオクタアルギニン[9]を付加し，細胞をピレンブチレートで前処理[10]することにより，NBDプ

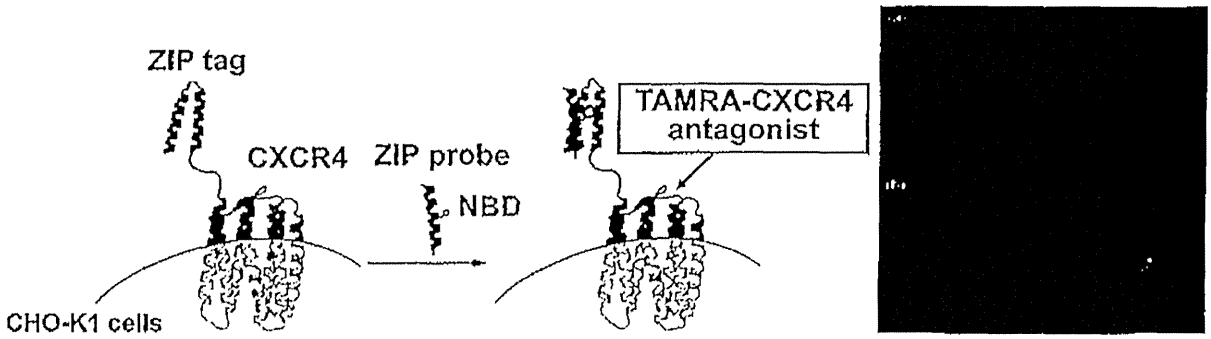

図3　ZIPタグ-プローブペアによるCXCR4の蛍光イメージング．ZIPタグをN末に融合したCXCR4発現CHO-K1細胞にNBDプローブとTAMRA標識CXCR4アンタゴニストを添加した(左図)．TAMRA標識CXCR4アンタゴニスト由来の赤色(a)とNBDプローブ由来の緑色(b)が共局在している(d)のがわかる(右図)

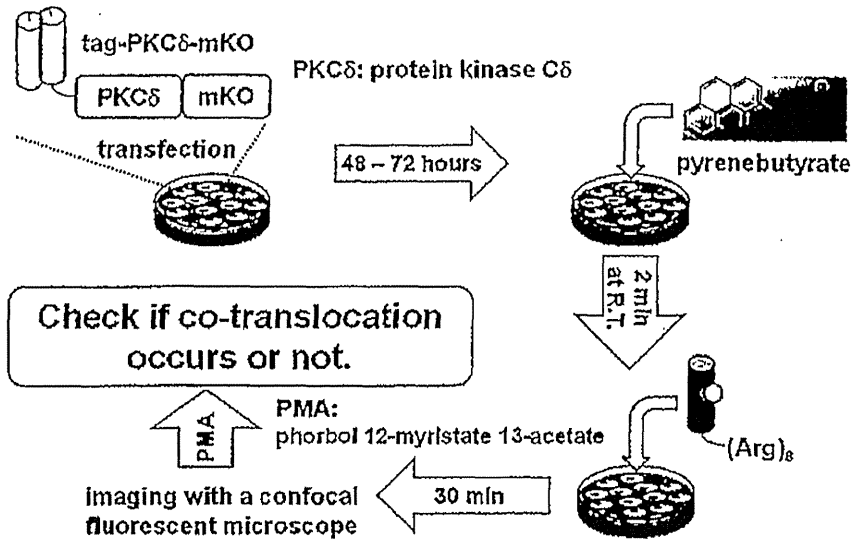

図4　ZIPタグ-プローブペアによるPKCδの蛍光イメージング．ZIPタグをN末に，KusabiraOrange (mKO)をC末に融合したPKCδ発現CHO-K1細胞に，ピレンブチレートとオクタアルギニン付加NBDプローブを添加し，共焦点顕微鏡で観察した．さらにPKCのリガンドであるphorbol 12-myristate 13-acetate (PMA)を添加し，PKC-タグ-プローブ-PMAのco-translocationを追跡した

ローブ分子を細胞内へ導入することができた．その結果，生細胞内のPKCを蛍光ラベル化して観察できた．また，PKCのリガンドであるphorbol 12-myristate 13-acetate (PMA)を添加することにより，PKC-タグ-プローブ-PMAのco-translocationを追跡することに成功した．このことにより，生細胞内においてリガンドによるタンパク質の動きを追跡できるほどZIPタグ-プローブペアは高い親和性と特異性で結合しており，高い蛍光応答能を持って機能することを示唆している．

5．ZIPタグ-プローブペアのまとめ

ZIPタグ-プローブシステムは，環境応答性色素としてNBDを採用し，ロイシンジッパー構造の逆平行3本鎖に基づくタグとプローブの選択的結合に伴って，蛍光波長・強度が大きく変化する生細胞上および生細胞内タンパク質のイメージングシステムである．これまでに，NBDに代わる色素として7-diethylaminocoumarin (DEAC)を導入し青色蛍光を発するプローブも開発しており[11]，また，タグとプローブを共有結合で架橋するクロス

リンク型のZIPタグ-プローブシステムも創出している[12]．これらは，今後，タンパク質イメージングのための有用なツールとなるであろう．

6．創薬ターゲットとしてのGタンパク質共役型受容体

7回膜貫通Gタンパク質共役型受容体(GPCR)は低分子医薬品の分子標的のうち約30%を占めており，重要な創薬ターゲットである[13]．近年，GPCRがホモあるいはヘテロの二量体化等の多量体化によってシグナル伝達を活性化する可能性が示唆されている[14]．GPCRは膜貫通型のタンパク質であるため，X線結晶構造解析はいくつか報告されているものの一般には非常に困難であることが知られている．そこで，GPCRの細胞膜表面での多量体化状態を検出することは機能解析において重要である．

7．ケモカイン受容体CXCR4

これまでわれわれは，GPCRに属するケモカイン受容体CXCR4に対するアンタゴニストの創製を精力的に行っている[15]．ケモカインは特定の白血球の遊走作用や活性化作用を有する一連のサイトカインの総称である．CXCR4はケモカインCXCL12/stromal cell-derived factor-1(SDF-1)を内因性リガンドとする受容体である[16]．CXCR4はCXCL12との相互作用により，胎生時の血管形成や心形成，造血，神経形成においてprogenitor cellの遊走や活性化等の重要な作用を示す．このCXCR4をGPCRの一例として，後で取り上げることとする．病態との関連では，CXCR4とCXCL12との相互作用は固形がんの転移，血液がんの進行，関節リウマチの炎症などに関与し[17]，また，CXCR4はヒト免疫不全ウイルス(human immunodeficiency virus，HIV)の感染の際に第二受容体(co-receptor)[18]として機能している．このようにCXCR4はさまざまな疾病に関与する創薬のmulti-targetとして注目されており，われわれは現在までに多数のCXCR4アンタゴニストの創製を行ってきた[15]．1980年代後半から京都大学藤井信孝研究室(玉村の前所属)では，カブトガニ血球由来の防御ペプチドpolyphemusinの構造活性相関研究を進め，18残基からなる侵入阻害ペプチドT22を見出した(図5)[19]．そして，CXCR4がHIV侵入のコレセプターとして同定されて以来，T22はCXCR4アンタゴニストであることが証明され[20]，構造最適化により14残基のCXCR4アンタゴニストT140を見出した[15]．生体内安定型T140誘導体は現在，臨床試験(phase II)中である[21]．また，T140のファルマコフォアのアミノ酸残基を基にした環状ペンタペプチドFC131を創出した[15]．これらのリード化合物をもとに低分子のペプチドミミック，非ペプチド性二核亜鉛錯体やその誘導体も創出している[22]．われわれがT22からT140誘導体へと構造最適化を進めている2000年代初頭に，CXCR4とCXCL12の相互作用が種々の固形がんの転移や血液がんの進行，関節リウマチの炎症等に関与することが明らか

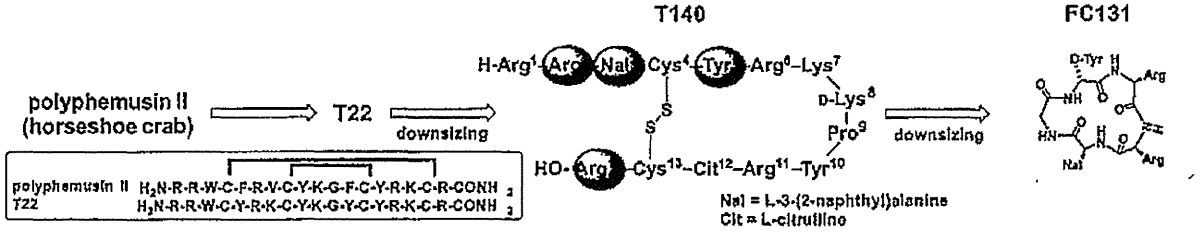

図5　カブトガニ血球由来の防御ペプチドpolyphemusinからペプチド性CXCR4アンタゴニストT140およびFC131の創製．T140中のグラデーションサークルは活性に重要なアミノ酸残基を示す

にされた[17]．それに伴い，T140誘導体ががん転移阻害活性，白血病の進行の阻害活性，抗関節リウマチ作用を有することも明らかにした[23]．CXCR4アンタゴニストの臨床応用においては，CXCR4とCXCL12の相互作用が生理的に重要な作用を示すことから，アンタゴニストの副作用を十分検討する必要がある．

8．2価型CXCR4リガンドのデザインと創製

種々のGPCRが多量体化することによってシグナル伝達を活性化する可能性が示唆されており，CXCR4も種々のがん細胞で過剰発現しており[24]，その二量体化ががんの悪性度，転移性に関与することが報告されている．CXCR4のリガンドを2価結合型とすることにより，CXCR4発現量に応じた細胞イメージングを可能とし，CXCR4が過剰発現した腫瘍細胞を特異的に認識することができないかと考えた．一般に2価型リガンドは単量体と違って結合の相乗的効果によって高い結合親和性を示す．これまでに創製されたGPCRの2価型リガンドの多くは，リガンドユニット間をつなぐリンカー部位においてアルキル鎖，もしくは水溶性を向上させるためにポリエチレングリコール鎖を用いていた．これらのリンカー構造は柔軟であり，標的である二量体GPCRに対して適合するような長さのリンカーを有するリガンドを合成することが困難であった．そこでわれわれは比較的堅固な構造を有するポリ-L-プロリン鎖を用いることによって，リガンドユニット間の距離を一定に固定化する構造をもつリガンドを創製した(図6)．これまでにポリ-L-プロリン鎖を活用した機能性分子はいくつか報告されているが，リガンド間の距離をポリプロリンによって固定化するという報告はなく，われわれの研究が初報である[25]．CXCR4リガンドとしてはFC131のグリシンをD-システインに置換したcFC131を用いた(図6(A))．Fmoc型固相合成法によって，6-27残基のポ

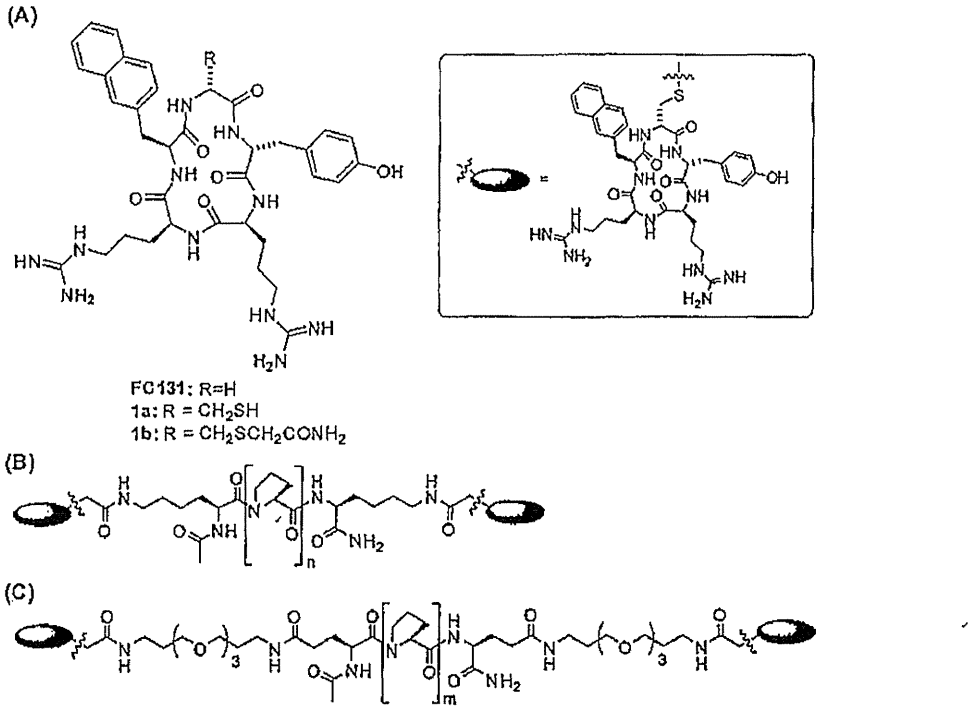

図6　(A)CXCR4リガンドFC131のコンジュゲート用誘導体cFC131(1a)とそのキャッピング誘導体(1b)．(B)ポリプロリンリンカーで架橋した2価型CXCR4リガンド(n＝6～27)．(C)ポリプロリン－PEGリンカーで架橋した2価型CXCR4リガンド(m＝3～18)

リプロリンリンカーを合成し，両末端にクロロアセチル基を導入した(図6(B))．また，ポリプロリンリンカーの両末端にポリエチレングリコール(PEG)を導入したリンカーも同時に合成した(図6(C))．そして，各リンカーに対してcFC131を導入し，結果的に2～8 nmの長さをカバーするリンカーを持つ2価型リガンドを合成した．ポリプロリンリンカーおよびポリプロリン-PEGリンカーを持つリガンドの両方において5.5～6.5 nmの長さのリンカーで最大のCXCR4結合活性を示した．すなわち，二量体CXCR4における結合ポケット間の距離がその長さに相当すると考えられる．ロドプシン構造を利用した二量体会合様式の推定においては，膜貫通ヘリックスtransmembrane region(TM)4とTM5が介した会合様式となり，FC131の結合ポケット間の距離と上述のリンカー長が一致した．2010年にCXCR4のX線結晶構造が報告されたが，この報告では結晶中においてはTM5とTM6が細胞質で相互作用する会合様式をとっている[26]．しかし，GPCRの会合様式としてはTM4とTM5を介する会合様式が一般的であり，結晶構造解析に用いられたCXCR4には大幅なアミノ酸変異が導入されていることから，細胞膜表面での会合様式を反映していない可能性も高い．この2価型リガンドを用いた解析によって得られたTM4とTM5の会合様式が信頼性の高いものである．

9．2価型リガンドを用いたCXCR4イメージングと腫瘍プローブへの応用

最適な2価型リガンドのポリプロリン$((Pro)_{18})$リンカー部位に蛍光基TAMRAを導入することにより，細胞表面上でのCXCR4に対する結合が可視化できるかどうかを検討した．まず，CXCR4のC末端にEGFPを融合したタンパク質を強制発現したHeLa細胞を用いて共焦点レーザー顕微鏡により観察した．その結果，2価型リガンドにおいては，リガンドのTAMRA由来の赤色蛍光とCXCR4の存在を示すEGFP由来の緑色蛍光との共局在が明瞭に見られた(図7，左)．単量体リガンドと比較することにより，2価型リガンドの選択性が確認された(図7，右)．また，CXCR4の発現量が異なる3種類の細胞(CXCR4発現量の多い順にJurkat, HeLa, K562)において，2価型リガンドではCXCR4の発現量に比例して結合量が増大すること，単量体ではそのような現象が見られないことを見出した．さらに，CXCR4の発現量が亢進しているヒト肺がん由来のA549と，成長因子FGFを除いて培養を行ったCXCR4の発現がほとんど見られないヒト血管上皮細胞HUVECを用いたイメージングを行い，A549では2価型リガンドで強い蛍光が検出でき，HUVECにおいてはバックグラウンド蛍光も確認されないことが示された．これらの結果は細胞表面でCXCR4発現量が増大すると，二量体化して存在するCXCR4の割合が増えるということを示唆している．この分子イメージング実験において，25 nMという非常に低いリガンド濃度で明瞭な分子イメージングが可能であるため，抗体(μMオーダーレベルで使用)などと比較しても優れたイメージング性能を有しているといえる．

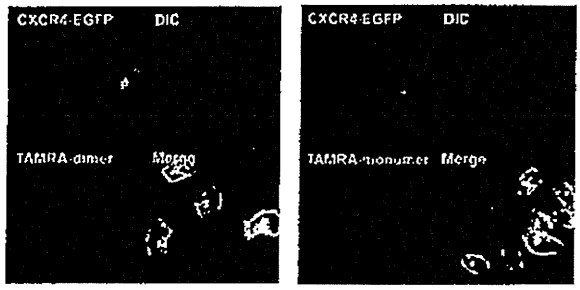

図7　TAMRA標識2価型CXCR4リガンド(左)および単量体リガンド(右)を用いたCXCR4-EGFP強制発現HeLa細胞のイメージング．2価型リガンド(25 nM)を用いた場合，単量体リガンド(50 nM)を用いた場合に比べ，明瞭なCXCR4との共局在が見られる．Barは50 μmを示す

10. 2価型CXCR4リガンドのまとめ

本研究では，ポリプロリンリンカーを用いて2価型CXCR4リガンドのユニット間を適切な距離に固定化する手法を見出した．これは他のGPCRリガンドにも広く応用が可能であると考えられ，本法によってX線結晶構造が未だに解かれていない種々のGPCRに関してその会合状態の推定やリガンド結合部位間の距離の推定が可能になると期待される．さらに，腫瘍認識プローブとしての2価型CXCR4リガンドの有用性を紹介した．2価型リガンドは診断薬としての展開が期待されるが，がん転移阻害剤としても有望なデータを得ており，双方への発展も視野に入れて進めている．

11. おわりに

本稿では，「ターゲットタンパク質を特異的に認識するプローブ」として，前半ではわれわれが開発したZIPタグ-プローブシステムを，後半では二量体GPCRを認識するプローブを紹介した．生命現象をより深く理解するために，生細胞におけるタンパク質の機能や局在，タンパク質間の相互作用を詳細に解析するためのツールが重要になる．われわれは他にも多くの有用なツールを開発しており，そのことによって，ケミカルバイオロジー研究，生命科学研究に貢献したいと考えている．本研究を遂行するにあたってお世話になりました，大橋南美機関研究員（講師相当），水口貴章助教，堤浩博士（現・東京工業大学助教），田中智博博士（現・東京理科大学研究員）をはじめ，東京医科歯科大学メディシナルケミストリー分野の職員および学生に感謝致します．

参考文献

1) Shimomura O, Johnson FH, Saiga Y. (1962) *J. Cell. Comp. Physiol.*, 59, 223-239
2) Griffin BA, Adams SR, Tsien RY. (1998) *Science*, 281, 269-272; Gaietta G, *et al.* (2002) *Science*, 296, 503-507
3) Gronemeyer T, Godin G, Johnsson K. (2005) *Biotechnol.*, 16, 453-458
4) Ojida A, *et al.* (2006) *J. Am. Chem. Soc.*, 128, 10452-10459
5) Tripet B, *et al.* (1996) *Protein Eng.*, 9, 1029-1042; Obataya I, *et al*, (2001) *Biopolymers*, 59, 65-71
6) Lobejoy B, *et al.* (1993) *Science*, 259, 1288-1293
7) Tsutsumi H, *et al.* (2009) *Angew. Chem. Int. Ed.*, 48, 9164-9166
8) Nomura W, *et al.* (2008) *Bioconjugate Chem.*, 19, 1917-1920
9) Futaki S, *et al.* (2001) *J. Biol. Chem.*, 276, 5836-5840
10) Takeuchi T, *et al.* (2006) *ACS Chem. Biol.*, 1, 299-303
11) Tsutsumi H, *et al.* (2011) *ChemBioChem*, 12, 691-694
12) Nomura W, *et al.* (2010) *Biopolymers. (Pep. Sci.)*, 94, 843-852
13) Overington JP, *et al.* (2006) *Nature Rev. Drug. Discov.* 5, 993-996
14) Wang J, *et al.* (2006) *Mol. Cancer Ther.* 5, 2474-2483
15) Tamamura H, *et al.* (1998) *Biochem. Biophys. Res. Commun.*, 253, 877-882; Fujii N, *et al.* (2003) *Angew. Chem., Int. Ed.*, 42, 3251-3253; Tamamura H, *et al.* (2005) *J. Med. Chem.*, 48, 3280-3289; Tanaka T, *et al.* (2008) *Org. Biomol. Chem.*, 6, 4374-4377
16) Nagasawa T, *et al.* (1994) *Proc. Natl. Acad. Sci. USA*, 91, 2305-2309
17) Koshiba T, *et al.* (2000) *Clin. Cancer Res.*, 6, 3530-3535; Müller A, *et al.* (2001) *Nature*, 410, 50-56; Kijima T, *et al.* (2002) *Cancer Res.*, 62, 6304-6311; Nanki T, *et al.* (2000) *J. Immunol.*, 165, 6590-6598
18) Feng Y, *et al.* (1996) *Science*, 272, 872-877
19) 玉村啓和, (1998) 最新医学, 53(9), 2040-2046
20) Murakami T, *et al.* (1997) *J. Exp. Med.*, 186, 1389-1393
21) Tamamura H, *et al.* (2003) *Org. Biomol. Chem.*, 1, 3656-3662; Tamamura H, *et al.* (2003) *Org. Biomol. Chem.*, 1, 3663-3669
22) Tamamura H, *et al.* (2006) *Org. Biomol. Chem.*, 4, 2354-2357; Tamamura H, *et al.* (2006) *J. Med. Chem.*, 49, 3412-3415; Tanaka T, *et al.* (2011) *ChemMedChem*, 6, 834-839
23) Tamamura H, *et al.* (2003) *FEBS Lett.*, 550, 79-83; Tamamura H, *et al.* (2004) *FEBS Lett.*, 569, 99-104
24) Balkwill F, *et al.* (2004) *Semin. Cancer Biol.*, 14, 171-179
25) Tanaka T, *et al.* (2010) *J. Am. Chem. Soc.* 132, 15899-15901
26) Wu B, *et al.* (2010) *Science*, 330, 1066-1071

Virology 460-461 (2014) 1–10

Contents lists available at ScienceDirect

Virology

journal homepage: www.elsevier.com/locate/yviro

Generation of a monkey-tropic human immunodeficiency virus type 1 carrying *env* from a CCR5-tropic subtype C clinical isolate

Hiroyuki Otsuki, Mai Yoneda, Tatsuhiko Igarashi, Tomoyuki Miura*

Laboratory of Primate Model, Experimental Research Center for Infectious Diseases, Institute for Virus Research, Kyoto University, 53 Shogoin Kawara-cho, Sakyo-ku, Kyoto 606-8507, Japan

ARTICLE INFO

Article history:
Received 25 December 2013
Returned to author for revisions
21 January 2014
Accepted 25 April 2014
Available online 27 May 2014

Keywords:
Monkey-tropic HIV-1
Pig-tailed macaque
Intracellular homologous recombination
Primary isolate
Subtype C
CCR5 tropism
in vitro passage
Animal model
AIDS
Restriction factor

ABSTRACT

Several derivatives of human immunodeficiency virus type 1 (HIV-1) that evade macaque restriction factors and establish infection in pig-tailed macaques (PtMs) have been described. These monkey-tropic HIV-1s utilize CXCR4 as a co-receptor that differs from CCR5 used by most currently circulating HIV-1 strains. We generated a new monkey-tropic HIV-1 carrying *env* from a CCR5-tropic subtype C HIV-1 clinical isolate. Using intracellular homologous recombination, we generated an uncloned chimeric virus consisting of at least seven types of recombination breakpoints in the region between *vpr* and *env*. The virus increased its replication capacity while maintaining CCR5 tropism after *in vitro* passage in PtM primary lymphocytes. PtM infection with the adapted virus exhibited high peak viremia levels in plasma while the virus was undetectable at 12–16 weeks. This virus serves as starting point for generating a pathogenic monkey-tropic HIV-1 with CCR5-tropic subtype C *env*, perhaps through serial passage in macaques.

Introduction

Nonhuman primate models with human-like immune systems are often employed to evaluate the efficacy of candidate vaccines against acquired immune deficiency syndrome (AIDS). However, human immunodeficiency virus type 1 (HIV-1) infects humans or chimpanzees (*Pan troglodytes*) but not rhesus macaques (*Macaca mulatta*), the most widely used primate species in biomedical research (Gibbs et al., 2007). Experimental infection of macaques with simian immunodeficiency virus (SIV) or simian-human immunodeficiency virus (SHIV) has been used extensively to investigate HIV-1 infection *in vivo*. Pathogenic infection with SIV allows insight into the mechanisms of pathogenesis and provides information for development of novel vaccination strategies. However, due to the marked antigenic difference in viral proteins between HIV-1 and SIV, macaque models with SIV are not suitable for evaluating the immune response directed against HIV-1 (Javaherian et al., 1992; Kanki et al., 1985; Murphey-Corb et al., 1986). SHIV, a chimeric virus carrying *tat, rev, vpu* and *env* from HIV-1 with an SIV genetic backbone, has been constructed and used widely to assess the immune response and pathogenicity directed against HIV-1 Env (Shibata and Adachi, 1992; Reimann et al., 1996; Harouse et al., 1999)

Highly pathogenic SHIV irreversibly depletes circulating $CD4^+$ T-lymphocytes, and cause rapidly AIDS-like symptoms in infected macaques. These properties are, however, different from the vast majority of circulating HIV-1 or SIV isolates, and the discrepancy would be attributed to the viral co-receptor preference (Nishimura et al., 2004). Entry of HIV-1 into cells is mediated through the interaction of viral envelope protein with cellular CD4 and subsequent binding to either the CCR5 or CXCR4 chemokine receptor or both receptors. The vast majority of HIV-1 clinical isolates preferentially utilize CCR5 as the co-receptor for entry (Choe et al., 1996). The CXCR4-tropic or dual-tropic viruses that utilize both CCR5 and CXCR4 emerge during late stages in the disease course (Doranz et al., 1996; Feng et al., 1996).

In addition to the co-receptor usage, it is necessary to consider the variation of *env* gene in SHIV construction. Most HIV-1 strains currently circulating belong to group M, consisting of subtypes A–D, F–H, J, K and their recombinants, and are largely responsible for the global AIDS pandemic (Hemelaar, 2012). Most of early SHIVs are generated by utilizing genes derived from subtype B

* Corresponding author. Tel.: +81 75 751 3984; fax: +81 75 761 9335.
E-mail address: tmiura@virus.kyoto-u.ac.jp (T. Miura).

http://dx.doi.org/10.1016/j.virol.2014.04.037
0042-6822/

viruses, which comprise an estimated 11% of the global prevalence of HIV-1. By contrast, subtype C is the dominant subtype, accounting for almost 50% of global infections. Subtype C viruses do not share the antigenicity of Env as the main target of neutralizing antibodies with subtype B viruses (Choisy et al., 2004; Gaschen et al., 2002). The V3 loop region of the subtype C envelope is less variable than that of other subtypes (Kuiken et al., 1999), and mutations appear to accumulate in the C3 and V4 regions, which are targets of autologous neutralizing antibody responses in individuals infected with subtype C viruses (Moore et al., 2008, 2009). The structure of these epitopes is dissimilar between subtypes B and C (Gnanakaran et al., 2007). There are pathogenic SHIVs that encode CCR5 tropic subtype C env gene (Ndung'u et al., 2001; Ren et al., 2013; Song et al., 2006).

Conventional SHIV that encodes SIV sequence in 5′ half of the genome has limited utility in the evaluation of cell-mediated immunity induced by a vaccine because it does not contain HIV-1 Gag in its genome; consequently, SHIV has different major epitopes for cytotoxic T lymphocytes (CTLs) known to be associated with lowering the plasma viral load in HIV-1 infection (Goulder and Watkins, 2004; Kiepiela et al., 2007). Recently, two major restriction factors were reported to block HIV-1 replication in monkey cells in a species-specific manner (Neil and Bieniasz, 2009). The restriction factor apolipoprotein B mRNA-editing enzyme-catalytic polypeptide-like 3G (APOBEC3G) protein is incorporated into viral particles and induces hypermutation in proviral DNA in target cells mediated by its cytidine deaminase activity (Sheehy et al., 2002). Macaque APOBEC3G proteins are counteracted by the SIV Vif protein but not by HIV-1 Vif (Mariani et al., 2003). The other major restriction factor that inhibits the viral replication cycle is tripartite motif 5α (TRIM5α) protein, which directly recognizes incoming viral capsid (CA) (Stremlau et al., 2004). HIV-1 CA can bind cyclophilin A (CypA), a ubiquitous cytosolic protein, to evade restriction by human TRIM5α, whereas the CypA-binding activity appears to enhance TRIM5α recognition in macaque cells (Berthoux et al., 2005; Keckesova et al., 2006; Stremlau et al., 2006). It is known that the host species barrier of Pig-tailed macaques (PtMs) (*Macaca nemestrina*) against HIV-1 is weaker than other macaques because they do not have the TRIM restriction (Brennan et al., 2008).

Based on these findings, derivatives of HIV-1 that has a remarkably different structure from the conventional SHIV were constructed by the introduction of minor genetic modifications into its genome to overcome the restriction factors in macaque cells. Hatziioannou et al. (2006) generated simian-tropic HIV-1 (stHIV-1) by replacing the entire *vif* gene of HIV-1 with that of SIVmac or HIV type 2. Kamada et al. (2006) reported the monkey-tropic HIV-1 (HIV-1mt) NL-DT5R, in which the CypA-binding motif of the CA protein is substituted by the corresponding sequence of SIVmac, and the entire *vif* gene is also substituted. Thippeshappa et al. (2011) generated HSIV-vif, a clone of HIV-1 by substituting the *vif* gene with that of a pathogenic SIVmne clone. These derivatives of HIV-1 established persistent infection in PtMs for months but were controlled thereafter (Hatziioannou et al., 2009; Igarashi et al., 2007; Thippeshappa et al., 2011). These monkey-tropic HIV-1 derivatives currently available are not CCR5-tropic; NL-DT5R and HSIV-Vif encode *env* from a CXCR4-tropic, and stHIV-1 encodes *env* from dual-tropic subtype B viruses.

In this study, we generated a new HIV-1mt strain carrying *env* from a CCR5-tropic subtype C HIV-1 clinical isolate. We employed intracellular homologous recombination (IHR) to produce the recombinant virus. Since the viral swarm generated by IHR did not show efficient replication in PtM primary cells, we conducted *in vitro* serial passages of the virus. Thus, we successfully generated a viral swarm that exhibited an enhanced replication capacity in PtM cells and established infection in PtMs with high peak viremia comparable to the currently available monkey-tropic HIV-1 derivatives.

Results

Generation of a new HIV-1mt carrying CCR5-tropic subtype C env through IHR

We employed IHR to generate recombinant viruses (Fujita et al., 2013). First, we prepared DNA fragments by polymerase chain reaction (PCR) amplification of a region spanning the 5′ long terminal repeat (LTR) to upstream of the V1/V2 region in *env* (nucleotide positions 1–6784 based on HXB2 numbering; accession number: K03455) using the plasmid DNA template encoding the full-length NL-DT5R proviral genome (fragment I in Fig. 1A). This fragment encodes a CypA-binding motif derived from the corresponding sequence of SIVmac239 to evade restriction from macaque TRIM5α, and the entire SIVmac239 *vif* gene to counteract the macaque APOBEC3G. Second, a region spanning the *vpr* gene to the R region of the 3′ LTR (nucleotide positions 5558–9625 based on HXB2 numbering) was amplified from the HIV-1 97ZA012 strain (fragment II in Fig. 1B). To increase the possibility to obtain a virus that can replicate in monkeys well, we thought that it was better to generate swarm viruses having variation without cloning. Resultant recombinant virus might fail to replicate normally if recombination occurred between fragments I and II that resulted in the 5′ LTR of subtype B and the 3′ LTR of subtype C. The discordance of the 3′ and 5′ LTR may disrupt successful translocation of the minus strand strong stop DNA to the plus strand genomic RNA during reverse transcription (Goff, 2007). To match the sequence of the 3′ LTR to that of the 5′ LTR, we prepared a third DNA fragment encoding a region spanning the 5′ LTR to the middle of *gag* (nucleotide positions 1–1433 based on HXB2 numbering) from the proviral DNA extracted from HIV-1 97ZA012-infected cells (fragment III in Fig. 1B). Fragments I and II

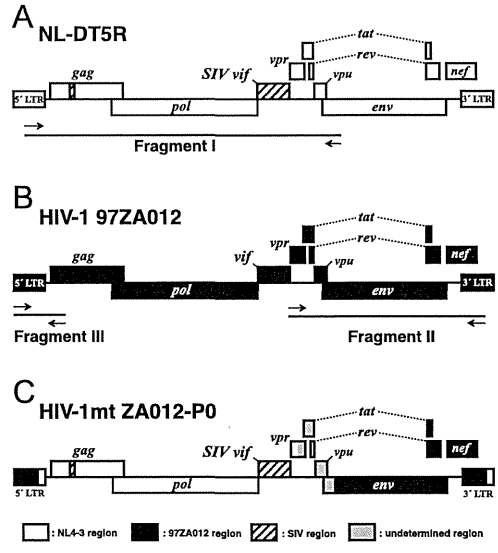

Fig. 1. Schematic representation of the genome organization of human immunodeficiency virus (HIV)-1 and monkey-tropic HIV-1 (HIV-1mt). Genome organizations of NL-DT5R (A), subtype C HIV-1 97Z012 (B) and HIV-1mt ZA012-P0 (C) are depicted. The horizontal line represents DNA fragments I, II and III, used for intracellular homologous recombination. Fragment I encodes a region from the 5′ LTR to *env* of NL-DT5R plasmid DNA. Fragment II encodes a region from the initiation of *vpr* to the R region of the 3′ LTR of the HIV-1 97ZA012 strain. Fragment III encodes a region from the 5′ LTR to upstream of the cyclophilin A-binding motif of the virus. Sequences from NL4-3 (open box), HIV-1 97ZA012 (filled box) and the SIVmac239 genome (diagonally striped box) are depicted. The gray box in HIV-1mt ZA012-P0 represents a gene that was not identified by direct sequence analysis.

had an overlapping region between the initiation of *vpr* to upstream of the *env* V1/V2 region, and fragments I and III had an overlapping region between the 5′ LTR to upstream of the CypA-binding site.

These amplified DNA fragments (fragments I, II and III) were co-transfected into C8166-CCR5 cells that are permissive to CCR5-tropic HIV-1. On day 8 post-transfection, we observed the formation of virus-induced cytopathic effects (CPEs), indicating the generation of replication-competent recombinant virus. The new recombinant virus was isolated and designated HIV-1mt ZA012-P0.

To determine the genomic organization of HIV-1mt ZA012-P0, we subjected the viral RNA isolated from the culture supernatant to direct sequencing. We found that the virus carried sequences of the U5 region of the 5′ LTR, *gag*, *pol* and *vif* derived from NL-DT5R and sequences of 3′ half of *env*, *nef*, and R and the U3 region of the 3′ LTR derived from 97ZA012 (Fig. 1C). First, the recombination breakpoint derived from fragments I and III was found to be located within the junction between the U5 and R region of the 5′ LTR (nucleotide positions 551–605 based on HXB2 numbering). However, additional recombination breakpoints between fragments I and II, encoding the *vpr–env* region, were not identified due to multiple peaks at the same locations in the analyzed sequence chromatograms. This result suggested that HIV-1mt ZA012-P0 represented a swarm that might contain several variants with various recombination breakpoints.

Increased replication competence of HIV-1mt ZA012 through long-term in vitro passage in CD8$^+$ cell-depleted pig-tailed macaque peripheral blood mononuclear cells (PBMCs)

We subsequently determined whether HIV-1mt ZA012-P0 replicates in CD8$^+$ cell-depleted pig-tailed macaque peripheral blood mononuclear cells (PtM PBMCs), in which the parental NL-DT5R replicated as described previously (Kamada et al., 2006). HIV-1mt ZA012-P0 from the culture supernatant of C8166-CCR5 was used to spinoculate CD8$^+$ cell-depleted PtM PBMCs, and the virion-associated reverse transcriptase (RT) activity was monitored in the culture supernatant (Fig. 2); however, no RT activity was detected in the culture supernatant after passage 1 (Fig. 2).

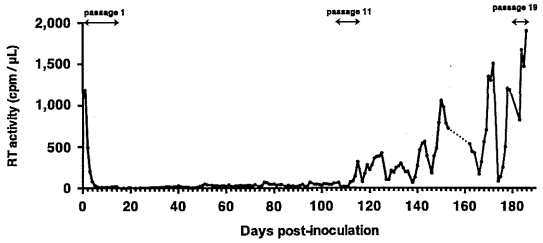

Fig. 2. Improved replication of HIV-1mt ZA012 throughout *in vitro* passages in CD8$^+$ cell-depleted PtM peripheral blood mononuclear cells (PBMCs). HIV-1mt ZA012-P0 was used to spinoculate CD8$^+$ cell-depleted PtM PBMCs, and virion-associated RT activity in the culture supernatant was monitored daily. Some of the infected cells were co-cultured with freshly prepared CD8$^+$ cell-depleted PtM PBMCs. One period of passage was indicated in the shaded grey or white zones. The dotted line indicates data not available.

Next we carried out *in vitro* serial passages to improve the replication competence of the virus as observed in the cases of HIV-1 (Freed and Martin, 1996; Willey et al., 1988). Infected cells were co-cultured with freshly prepared CD8$^+$ cell-depleted PtM PBMCs every 1 or 2 weeks. Although detectable RT activity was not observed during 10 successive passages (passage 1–10), a low level of viral replication was confirmed by the CPEs of C8166-CCR5 cells co-cultured with PBMCs taken from the passage (data not shown). A detectable peak of viral replication (319 cpm/μL) was observed at 115 days after the first inoculation (passage 11), and replication was maintained following passages, eventually resulting in enhanced replication in PtM PBMCs (1900 cpm/μL in passage 19). The resultant virus, isolated from the culture supernatant of passage 19, was designated HIV-1mt ZA012-P19.

To evaluate the replication capacity of the virus, the replication kinetics of HIV-1mt ZA012-P19 were compared to those of the parental NL-DT5R and HIV-1mt ZA012-P0. Each viral stock was normalized by the number of infectious units per cell (in this case, a multiplicity of infection (MOI) of 0.1) and used to inoculate CD8$^+$ cell-depleted PtM PBMCs isolated from two donor monkeys; virion-associated RT activity in the culture supernatant was monitored daily (Fig. 3). Although HIV-1mt ZA012-P19 exhibited a lower level of viral replication compared to that of SIVmac239, the virus showed more efficient replication than NL-DT5R and HIV-1mt ZA012-P0 in cells from both animals. Therefore, we successfully improved the replication capacity of the new HIV-1mt in PtM PBMCs by *in vitro* passaging.

Sequence analysis of HIV-1mt ZA012-P0 and ZA012-P19

It is likely that HIV-1mt ZA012-P0 acquired genetic changes and evolved to HIV-1mt ZA012-P19 through the serial passages in PtM PBMCs. To compare the genomic sequence of these viruses, we first performed single genome amplification (SGA) of viral RNA isolated from the culture supernatant to determine the nucleic acid sequences of the *vpr–env* region (nucleotide positions 5559–8795 based on HXB2) of HIV-1mt ZA012-P0. Subsequently, we identified the sequence of the region containing the expected recombination breakpoints generated by IHR between fragments I and II. Genetic analysis of 17 SGA clones revealed that these sequences had NL-DT5R sequences in the 5′ end and HIV-1 97ZA012 sequences in the 3′ end, with seven different recombination

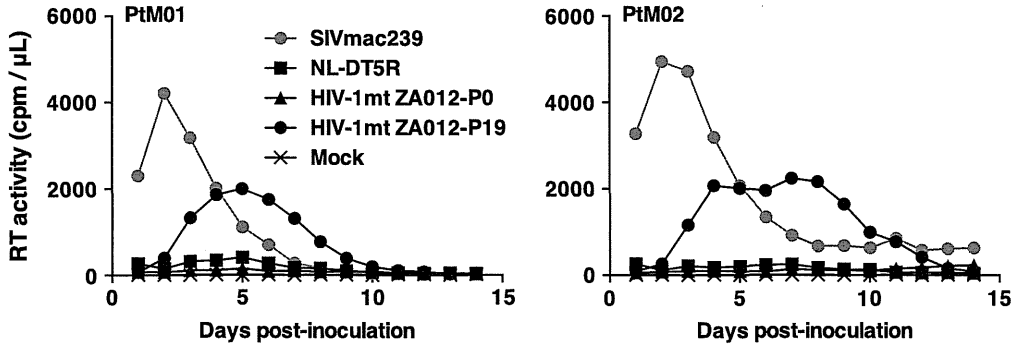

Fig. 3. Growth kinetics of HIV-1mt ZA012 in CD8$^+$ cell-depleted PtM PBMCs. Growth kinetics of HIV-1mt ZA012-P0, HIV-1mt ZA012-P19, SIVmac239 and NL-DT5R were compared in PBMCs from two PtMs. Each virus was used to spinoculate CD8$^+$ cell-depleted PtM PBMCs (MOI=0.1 $TCID_{50}$ per cell), and the virion-associated RT activity in the culture supernatant was monitored. The figure shown is representative of four independent experiments.

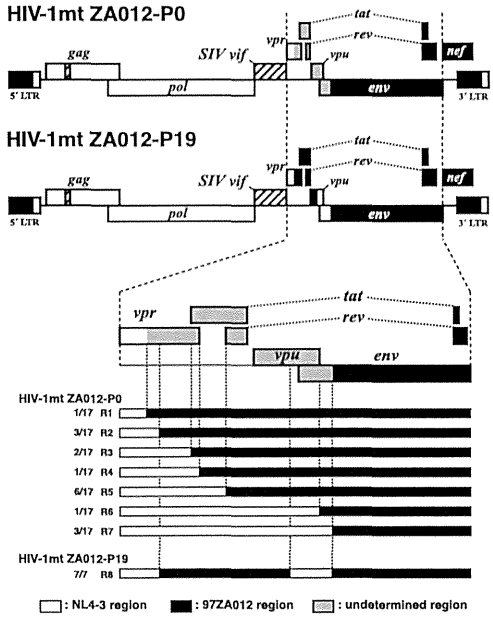

Fig. 4. Recombination breakpoints in HIV-1mt ZA012-P0 and ZA012-P19 genomes. The genome organizations of HIV-1mt ZA012-P0 and HIV-1mt ZA012-P19 are schematically represented (upper two diagrams). The region from the initiation of *vpr* to the end of *env* that included recombination breakpoint sites is depicted in the third diagram; the HIV-1mt ZA012-P0 (17 SGA sequences) or HIV-1mt ZA012-P19 (seven SGA sequences) are depicted (bottom). Sequences from HIV-1mt ZA012-P0 were classified into seven patterns of recombination breakpoints (R1 to R7). Sequences from HIV-1mt ZA012-P19 were classified into one recombination breakpoint pattern (R8). The numbers (left) indicate the numbers of sequences per analyzed sequence.

breakpoints in the region (Fig. 4). One recombination breakpoint was detected at nucleotide positions 178–187 of the *vpr* gene in 1/17 SGA sequences (5736–5745 in HXB2 numbering, recombination type R1) with 10 identical base pairs between NL-DT5R and 97ZA012. In addition to R1, we identified the following recombination types: the *vpr* gene in 3/17 SGA sequences (5760–5767; R2), the initiation of *tat* in 2/17 SGA sequences, (5821–5839; R3), the end of the *vpr* gene in 1/17 SGA sequence (5852–5865; R4), the initiation of *rev* in 6/17 SGA sequences (5960–6000; R5), the end of the *vpu* gene in 1/17 SGA sequence (6357–6392; R6) and the upstream of V1/V2 of the *env* gene in 3/17 SGA sequences (6467–6491; R7). These results suggest that homologous recombination occurs in various sites with homologous sequences.

Next, seven SGA sequences were amplified from viral RNA isolated from the culture supernatant of PtM PBMCs infected with HIV-1mt ZA012-P19, and nucleotide sequences and recombination breakpoints were determined in the same manner. Unexpectedly, all the sequences of HIV-1mt ZA012-P19 had three recombination breakpoints in the region from the *vpr* to *env* genes (recombination type R8 in Fig. 4). The first breakpoint was located in the *vpr* gene (5760–5767), the second was located in the *vpu* gene (6194–6213), and the third was located in *env* (6467–6491) with the N-terminal portion of C1 region from NL4-3 sequence. Although the pattern of recombination breakpoint of the virus differed from those of HIV-1mt ZA012-P0, the first and third recombination breakpoints were identical to the recombination type of R2 and R7, respectively (Fig. 4). It is likely that HIV-1mt ZA012-P19 was generated from further recombination events that occurred in the middle of the *vpu* gene (6194–6213) between recombination type R2 and R7 of HIV-1mt ZA012-P0.

It is conceivable that the genome of HIV-1mt ZA012-P19 acquired several amino acid mutations associated with the enhanced replication in PtM PBMCs. Compared with the deduced amino acid sequences in HIV-1mt ZA012-P0, HIV-1mt ZA012-P19 acquired substitutions from Lys to Arg at amino acid position 432 in Pol-RT and Asp to Glu at position 232 in Pol-IN that were in the NL-DT5R backbone. In addition, an amino acid substitution from Phe to Ser at 139 in Nef was found in HIV-1mt ZA012-P19 compared to 17 SGA sequences derived from HIV-1mt ZA012-P0. No nonsynonymous substitutions were identified in Gag and Vif, the proteins responsible for evading TRIM5α and APOBEC3. Around the recombination break points in HIV-1mt ZA012-P19, the *vpr* and *vpu* genes keep each open reading frame and do not contain any mutations in the region derived from NL-DT5R, respectively. Furthermore, consensus amino acid sequence of HIV-1mt ZA012-P0 and -P19 were also identical in the regions derived from HIV-1 97ZA012, respectively. These facts suggest that recombination was occurred to keep these genes intact.

Phylogenetic analysis of env genes

It is likely that HIV-1mt ZA012-P0 generated by IHR in human C8166-CCR5 cells was a swarm carrying diverse *env* sequences of the parental HIV-1 97ZA012, which evolved to HIV-1mt ZA012-P19 through *in vitro* passages. To evaluate the *env* variants selected in C8166-CCR5 cells or primary PtM cells, we determined 22 sequences of HIV-1 97ZA012, 17 sequences of HIV-1mt ZA012-P0

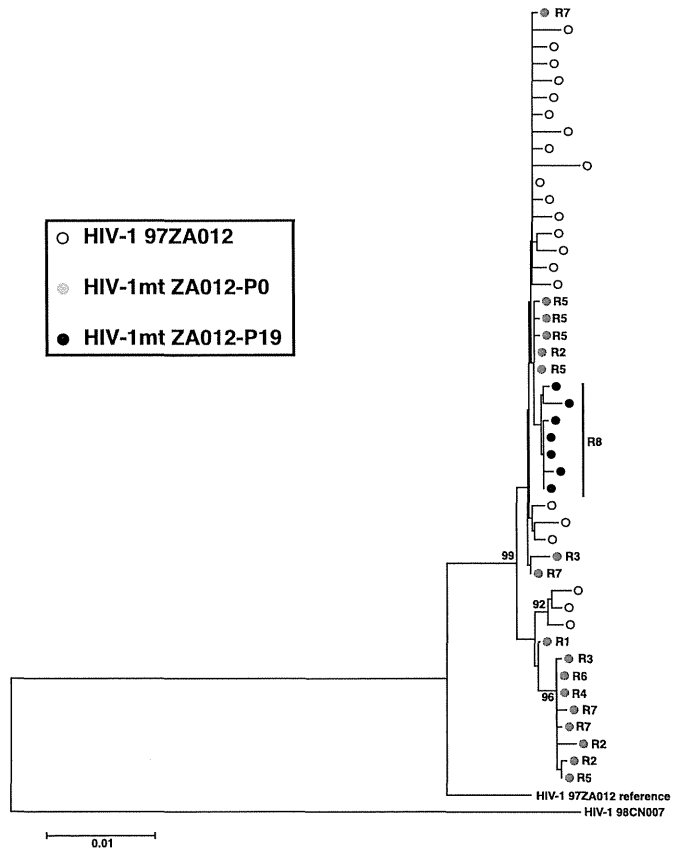

Fig. 5. Phylogenic analysis of partial *env* sequences. A neighbor-joining phylogenic tree was constructed from the partial nucleic acid sequences of *env* (nucleotide positions 211–2571 based on *env* of HXB2 numbering). The sequences of HIV-1 97ZA012 (white circle), HIV-1mt ZA012-P0 (grey circle) and HIV-1mt ZA012-P19 (black circle) were determined from SGA sequences. HIV-1 97ZA012 (accession number: AF286227) and 98CN007 (AF286230) reference sequences were obtained from the Los Alamos HIV sequence database (http://hiv-web.lanl.gov/). R1–R8 correspond to the patterns of recombination breakpoint types in Fig. 2. Bootstrap values were computed from 1000 bootstrap replicates, and only > 90% are shown at branches. The scale bar indicates the substitutions per site.

and seven sequences of HIV-1mt ZA012-P19 from SGA. Next, we conducted a phylogenetic analysis of the nucleotide sequences of the 3′ terminal 2361 bp of each viral *env* derived from HIV-1 97ZA012 and shared by all variants of HIV-1mt ZA012-P0 and -P19 (Fig. 5). These sequences were divided into two clusters: the larger cluster included 19 sequences of HIV-1 97ZA012, 8 sequences of HIV-1mt ZA012-P0 and 7 sequences of HIV-1mt ZA012-P19; and the smaller cluster included 3 sequences of HIV-1 97ZA012 and 9 sequences of HIV-1mt ZA012-P0. Recombination types R2, R3, R5 and R7 (Fig. 4) were intermingled among the sequences of the two groups, suggesting that homologous recombination could occur in various *env* templates.

To compare the genetic diversity of *env* in these viruses, we computed the mean of all pair-wise distances between any two viral *env* sequences in each of the viruses. The computed diversity of *env* in HIV-1mt ZA012-P0 was 0.0038 ± 0.0025 ($\pm$ standard deviation, SD), which was significantly lower than that in the parental HIV-1 97ZA012 (0.0044 ± 0.0021; $p < 0.05$). The computed diversity of HIV-1mt ZA012-P19 *env* was 0.0012 ± 0.00078, which showed significantly lower variation compared to HIV-1mt ZA012-P0 ($p < 0.0001$).

Co-receptor usage of HIV-1mt ZA012-P19

To characterize co-receptor usage of HIV-1mt ZA012-P19 after long-term *in vitro* passage, we conducted an entry assay using TZM-bl cells with small molecule antagonists (Fig. 6). Viral infectivity of the CXCR4-tropic virus (NL4-3) was reduced in the presence of an increasing amount of the CXCR4 inhibitor, AMD3100, but was not affected by the CCR5 inhibitor, AD101. In contrast, the CCR5-tropic virus, SIVmac239, was inhibited in the presence of an increasing amount of AD101 but not by AMD3100. Similar to the results using SIVmac239, HIV-1mt ZA012-P19 exhibited sensitivity to inhibition by AD101 but resistance to AMD3100, indicating that the virus maintained its CCR5-tropism after the serial passage.

Replication of HIV-1mt ZA012 in pig-tailed macaques

Since HIV-1mt ZA012-P19 utilized CCR5 as a co-receptor and exhibited increased infectivity to primary cells of PtMs, we next assessed the *in vivo* replication capacity of the virus by experimental infection of PtMs. Two PtMs were inoculated intravenously

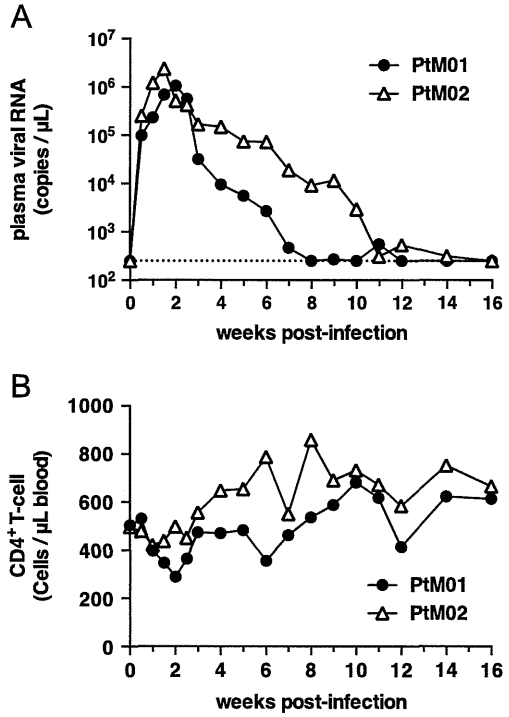

Fig. 7. HIV-1mt ZA012 infection of pig-tailed macaques. Two pig-tailed macaques were inoculated intravenously with HIV-1mt ZA012 (100,000 $TCID_{50}$), and the plasma viral RNA burdens (A) and circulating $CD4^+$ T-lymphocytes (B) were monitored.

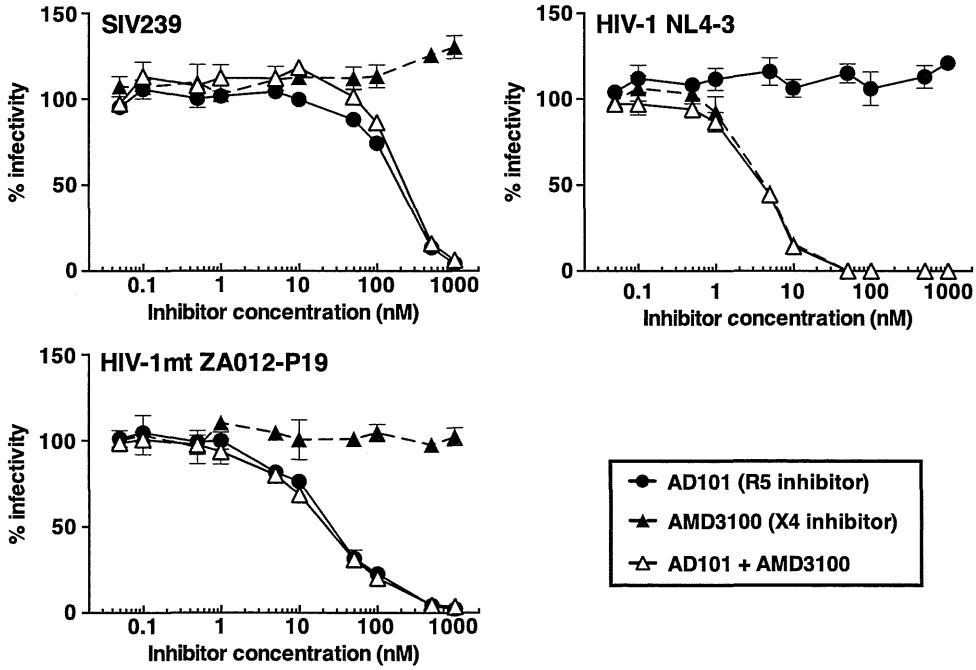

Fig. 6. Co-receptor usage of HIV-1mt ZA012-P19. Infectivity of HIV-1 NL4-3, SIVmac239 and HIV-1mt ZA012-P19 to TZM-bl cells was assessed in the presence of increasing amounts of AMD3100 (CXCR4 inhibitor), AD101 (CCR5 inhibitor) or both. The experiment was conducted in triplicate.

with 1.0×10^5 $TCID_{50}$ of the HIV-1mt prepared in PtM PBMCs, and plasma viral RNA burdens and the numbers of circulating $CD4^+$ T-lymphocytes were monitored periodically (Fig. 7A). Plasma viral RNA loads in PtM01 peaked (1.0×10^6 copies/mL) at 2 weeks post-infection (wpi) and declined thereafter to levels below the detection limit at 8 wpi. PtM02 exhibited a peak plasma viral RNA burden (2.3×10^6 copies/mL) at 1.5 wpi and maintained more than 1×10^4 copies/mL by 9 wpi, but the viral load declined to levels below the detection limit at 16 wpi. The numbers of $CD4^+$ T-lymphocytes in the circulation in both animals were not affected (Fig. 7B). Furthermore, we analyzed naive and memory populations of $CD4^+$ T cells and no preferential depletion of circulating memory $CD4^+$ T-lymphocyte was observed (data not shown).

Discussion

In this study, we used IHR to generate a new HIV-1mt carrying *env* from the CCR5-tropic subtype C HIV-1 clinical isolate. This recombination method has been used to generate infectious HIV-1 or SHIV by joining two linear DNAs in regions with completely identical sequences (Chen et al., 2000; Kalyanaraman et al., 1988; Kellam and Larder, 1994; Luciw et al., 1995; Srinivasan et al., 1989; Velpandi et al., 1991). Recently, we applied IHR to generate a replication-competent SHIV carrying subtype C *env* that was inserted within the *env* sequence of subtype B (Fujita et al., 2013). Here, we utilized the same method to generate HIV-1mt by replacing a coding sequence region from subtype B with that of a primary isolate of subtype C and investigated recombination breakpoints in detail by analyzing the sequences of the resultant viruses. We found seven variants with different recombination breakpoints that were located within overlapped sequences between fragments I and II. These variants were selected as replication-competent virus in C8166-CCR5 cells that maintained their variability, suggesting that IHR events occur frequently in cells co-transfected with DNA fragments. In addition, it appears that the length of identical sequence of as short as 8 bp is sufficient for IHR (recombination type R2 in Fig. 4). Furthermore, IHR is suggested to occur between various DNA templates, based on the phylogenetic analysis results that indicated intermingled types of recombination breakpoints among different *env* sequences.

To develop a virus that efficiently infects monkey cells, it is important to choose an *env* that mediates efficient entry to macaque cells. The Env proteins in most A–D subtypes of HIV-1 clinical isolates from infected individuals during the acute phase of infection do not mediate efficient entry using macaque CD4 receptors (Humes et al., 2012). In a preliminary experiment in C8166-CCR5 cells, we generated five strains of replication-competent HIV-1mt carrying *env* from subtype C HIV-1 clinical isolates, including 97ZA012, but only three were infectious to PtM cells (data not shown). The generation of SHIV 97ZA012 that can establish infection in rhesus macaques as described previously (Fujita et al., 2013) also suggested that Env of HIV-1 97ZA012 can generate recombinant viruses that are infectious to macaque cells.

The serial passage of HIV-1mt ZA012-P0 through PtM PBMCs resulted in the loss of variants with recombination breakpoints and led to the emergence of HIV-1mt ZA012-P19 variants with shared uniform mosaic breakpoints not detected before the passage (Fig. 4). It is possible that recombination type R8 was generated through additional recombination events within homologous sequences in the *vpu* region between variants with recombination type R2 and R7 because recombinant breakpoints located on *vpr* and *env* regions of the virus were identical to that of R2 and R7, respectively. This possibility of recombination between R2 and R7 is also supported by the previous finding that the AAAAA tract within the putative site of recombination is a recombination hotspot during reverse transcription because the sequence facilitates template switching by pausing and dissociation of reverse transcriptase and results in frequent recombination (Quinones-Mateu et al., 2002).

HIV-1mt ZA012-P19 acquired three amino acid substitutions (K432R of Pol-RT, D232E of Pol-IN and F138S of Nef) through serial passages in PtM PBMCs, but the biological significance of these mutations remains undetermined. It has been reported previously that two amino acid substitutions (N222K and V234I) in the C-terminus of Pol-IN of NL4-3 could augment replication of HIV-1mt in cynomolgus macaque HSC-F and human MT4/CCR5 cells (Nomaguchi et al., 2013). A D232E mutation observed in this study was positioned near these two residues, which might be associated with increased replication in primate cells.

HIV-1mt ZA012 established infection in PtMs with the peak viremia reaching $1.0–2.3 \times 10^6$ copies/mL at 1.5 or 2 wpi (Fig. 7). In contrast, NL-DT5R exhibited low levels of replication in PtMs (at most 3.5×10^4 copies/mL at peak viremia) regardless of $CD8^+$ cell-depletion, as described previously (Igarashi et al., 2007). Plasma viral RNA load at peak viremia in HSIV-vif infected newborn PtMs showed $0.5–1.0 \times 10^5$ copies/mL (Thippeshappa et al., 2011). The highest peak viral level has been achieved by stHIV-1 infection of PtMs, reaching $1.0 \times 10^5–10^6$ copies/mL at the peak (Hatziioannou et al., 2009). Although HIV-1mt ZA012 failed to persist its replication over 10 weeks, the replication capacity of the virus in the acute phase appeared to be comparable to or greater than known monkey-tropic HIV-1 isolates. The caveat is that HIV-1mt ZA012 was obtained through "autologous" cell passage.

The derivative of NL-DT5R was designed to counteract or evade restrictions by macaque TRIM5α and APOBEC3G but not by interferon (IFN)-stimulated genes (ISGs). One of the IFNα-inducible host factors, tetherin, inhibits release of viral particles from infected cells (Neil et al., 2008). HIV-1 Vpu is able to counteract human tetherin activity but fails to downregulate this activity in macaque (Jia et al., 2009). On the other hand, unlike HIV-1 HXB2 or NL4-3, some strains of HIV-1 appear to antagonize macaque tetherin by its N-terminal transmembrane (TM) domain of Vpu (Shingai et al., 2011). It has been reported that replication of monkey-tropic HIV-1 could be controlled in macaque lymphocytes treated with IFN-α (Bitzegeio et al., 2013; Thippeshappa et al., 2013). Further investigations are required to determine whether HIV-1mt ZA012-P19 that encodes the N-terminal TM domain of Vpu, Env and Nef from subtype C could efficiently replicate in the presence of PtM tetherin or ISGs.

We generated the first CCR5-tropic HIV-1mt in the currently available derivatives of HIV-1 that can establish infection in macaques. NL-DT5R, HSIV-vif and stHIV-1 are infectious to PtMs, but these viruses are CXCR4 or CXCR4/CCR5 dual tropic. Several monkey-tropic HIV-1 isolates carrying CCR5-tropic *env* have been reported, but the viral replication was less efficient than NL-DT5R (Yamashita et al., 2008). The CCR5-tropic viruses preferentially infect memory $CD4^+$ T-lymphocytes and efficiently replicate in effector sites *in vivo* (i.e., lymphocytes in the lung or gastrointestinal tract) (Brenchley et al., 2004; Mehandru et al., 2004; Okoye et al., 2007; Picker et al., 2004). Although we characterized co-receptor usage of HIV-1mt ZA012-P19 *in vitro*, further investigation is needed to determine whether the virus behaves similarly to CCR5-tropic HIV-1 isolates in patients *in vivo*.

In this study, we generated a new monkey-tropic HIV-1. The viral swarm HIV-1mt ZA012-P19 carries *env* sequences from CCR5-tropic subtype C HIV-1, and it successfully established infection in PtMs with a high peak viremia comparable or greater than the monkey-tropic HIV-1 strains currently available. Although the monkey-tropic HIV-1 requires further adaptation to improve its *in vivo* replication capacity, the virus potentially serves as a nonhuman primate model for AIDS, which reproduces infection with currently circulating HIV-1.